Article

Current Biology

Fatal accidents in neonatal pterosaurs and selective sampling in the Solnhofen fossil assemblage

Highlights

- Humeral fractures in neonatal *Pterodactylus* suggest injuries sustained during flight
- Injuries were caused by the storms that buried these and numerous other small pterosaurs
- Catastrophic storm sampling explains marked juvenile preservation bias in Solnhofen
- Large pterosaurs are rare or fragmentary due to low background attritional sampling

Authors

Robert S.H. Smyth, Rachel Belben, Richard Thomas, David M. Unwin

Correspondence

rabsmythpalaeo@gmail.com

In brief

Smyth et al. report wing injuries in neonatal pterosaurs from the Upper Jurassic Solnhofen assemblage, likely caused by storm events and supporting precocial flight ability. Taphonomic analysis reveals predominantly storm-driven mortality and a strong juvenile sampling bias across most Solnhofen pterosaurs, highlighting how local environmental conditions distort the fossil record.

Smyth et al., 2025, Current Biology *35*, 1–14
October 6, 2025
https://doi.org/10.1016/j.cub.2025.08.006

CellPress

Please cite this article in press as: Smyth et al., Fatal accidents in neonatal pterosaurs and selective sampling in the Solnhofen fossil assemblage, Current Biology (2025), https://doi.org/10.1016/j.cub.2025.08.006

Current Biology

CellPress
OPEN ACCESS

Article

Fatal accidents in neonatal pterosaurs and selective sampling in the Solnhofen fossil assemblage

Robert S.H. Smyth,[1,4,*] Rachel Belben,[1] Richard Thomas,[2] and David M. Unwin[3]
[1]Centre for Palaeobiology and Biosphere Evolution, School of Geography, Geology and the Environment, University of Leicester, Bennett Building, University Road, Leicester LE1 7RH, UK
[2]School of Heritage and Culture, University of Leicester, Kathleen Kenyon Building, University Road, Leicester LE1 7RH, UK
[3]Centre for Palaeobiology and Biosphere Evolution and School of Heritage and Culture, University of Leicester, Kathleen Kenyon Building, University Road, Leicester LE1 7RH, UK
[4]Lead contact
*Correspondence: rabsmythpalaeo@gmail.com
https://doi.org/10.1016/j.cub.2025.08.006

SUMMARY

The Upper Jurassic Solnhofen Archipelago of Germany has yielded a pterosaur assemblage that has long underpinned and continues to dominate much of our understanding of these flying reptiles. Knowledge of how this assemblage was shaped by processes of fossilization, critical for generating robust paleobiological hypotheses, remains limited. Here, we combine fatal trauma case studies with quantitative taphonomic data to reveal two distinct fossilization pathways. Catastrophic storms played a primary role, preferentially sampling small, immature pterosaurs. Storms caused these pterosaurs to drown and rapidly descend to the bottom of the water column, where they were quickly buried in storm-generated sediments, preserving both their skeletal integrity and soft tissues. Among these storm-sampled individuals, we document two highly immature specimens of *Pterodactylus* exhibiting similar oblique humeral fractures. These fractures are consistent with excessive wing loading during flight, providing compelling evidence of super-precocial flight capabilities in immature pterosaurs. By contrast, background "attritional" sampling under normal environmental conditions was less influential in generating the Solnhofen pterosaur assemblage. Longer residence times in the water column under normal environmental conditions restricted fossilization of larger pterosaurs, which are typically preserved as fragmentary, disarticulated remains lacking fossilized soft tissues. This bimodal taphonomic model reveals clear size- and taxon-related preservation biases, illustrating how extreme weather events can distort the fossil record. Selective sampling provides a framework for understanding the conditions that favored exceptional soft tissue preservation and offers critical context for evaluating pterosaur growth, flight capabilities, and paleoecology.

INTRODUCTION

The Upper Jurassic Solnhofen platy limestones of southern Germany (~153–148 mya) have yielded more than 500 examples of pterosaurs over the last 250 years.[1–4] Many specimens are complete, or near complete, and early finds formed the basis of our current understanding of pterosaur skeletal anatomy.[1,2,5–7] Much of our knowledge of pterosaur soft tissues, including throat-sacs,[8,9] tail vanes,[10] and the shape and structure of the wing membranes,[11–15] is derived from Solnhofen specimens, several of which are among the most informative of all pterosaurs.[9–11,14,16]

The Solnhofen assemblage is taxonomically diverse, comprising some 15 species representing at least six distinct lineages, including non-pterodactyliform, basal pterodactyliform, and pterodactyloid clades.[17,18] These pterosaurs have provided a crucible for testing approaches to pterosaur taxonomy[1,2,19–26] and are the principal contributors to character state data for most phylogenetic analyses of pterosaurs.[26] Several taxa, notably *Rhamphorhynchus muensteri* and *Pterodactylus antiquus*, are represented by relatively continuous postnatal growth series that include neonatal individuals,[21,26,27] likely no more than a few weeks old but capable of flight,[6,28,29] though this idea has been challenged.[27,30,31] Solnhofen pterosaurs have also been principal contributors of data to morphometric analyses[26,32–35] as well as studies of feeding ecology.[36] They are often treated as a classic example of a pterosaur "fauna," though the term is misleading, as the assemblage spans several million years and, as argued here, likely contains autochthonous and allochthonous elements.

Preservational biases, though rarely acknowledged, played a fundamental, yet poorly understood role, in shaping all aspects of the paleobiological studies mentioned above. Several generalized taphonomic pathways have been muted,[1,37–41] but there is little consensus as to which best accounts for the formation of the Solnhofen tetrapod assemblage. Taphonomic study

Please cite this article in press as: Smyth et al., Fatal accidents in neonatal pterosaurs and selective sampling in the Solnhofen fossil assemblage, Current Biology (2025), https://doi.org/10.1016/j.cub.2025.08.006

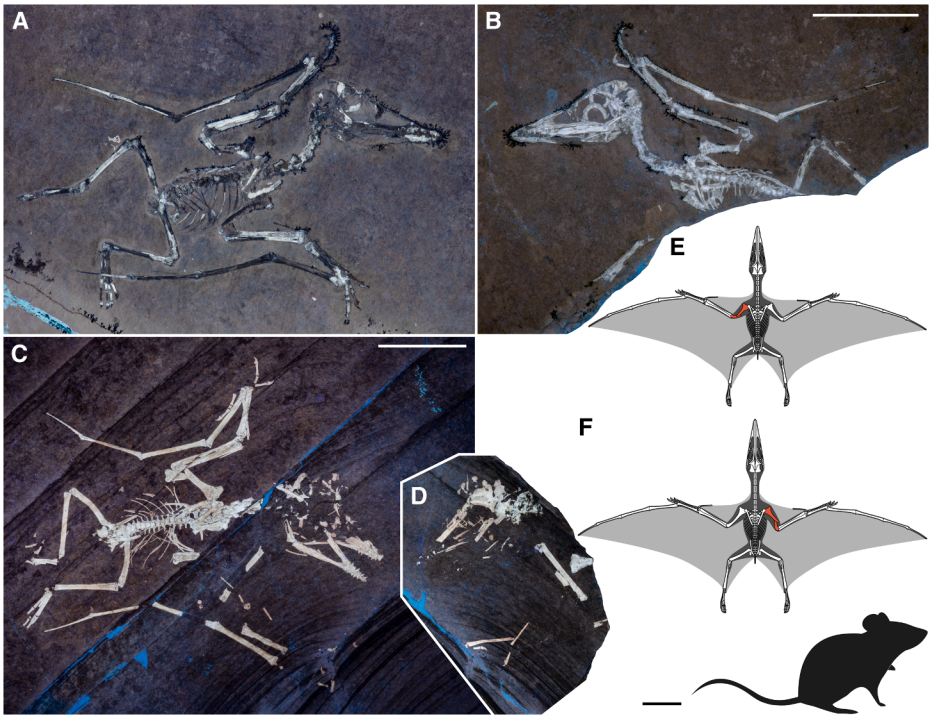

Figure 1. Neonatal examples of *Pterodactylus antiquus* displaying perimortem wing fractures

(A and B) Counterpart and part of MBH 250624-07 photographed under UV light, showing the broken left humerus in predominantly ventral view, with the skull exposed in lateral view.

(C and D) Part and counterpart of SNSB-BSPG 1993 XVIII 1508 a/b, photographed under UV light in ventral view, showing a fractured right humerus.

(E and F) Skeletal reconstructions of MBH 250624-07 (E) and SNSB-BSPG 1993 XVIII 1508 (F) depicted in a flight pose (plan view), with fractured elements highlighted in red, alongside the silhouette of a house mouse (*Mus musculus*) for scale.

Scale bars: 20 mm.

focused on Solnhofen pterosaurs remains limited.[1,42,43] Observations on soft tissue preservation are scattered across the literature,[11,14,16] but there have been no comprehensive systematic accounts. Consequently, in the absence of a coherent taphonomic model for the Solnhofen pterosaur assemblage, paleobiological hypotheses, especially those pertaining to soft tissue anatomy, ontogeny, and paleoecology, remain unconstrained and susceptible to misinterpretation.

Here we report two previously undescribed neonates of *Pterodactylus antiquus*, both exhibiting perimortem forelimb fractures. These specimens, together with quantitative data from over 40 individuals of *Pterodactylus*, offer new insights into two distinct taphonomic modes (catastrophic and attritional) that account for the preservation patterns observed in Solnhofen pterosaurs. To test the broader applicability of this model, we also conducted quantitative analyses of other abundant and well-sampled Solnhofen pterosaur groups: ctenochasmatoid pterodactyloids closely related to *Pterodactylus* and the more basal, non-pterodactyloid *Rhamphorhynchus*. Our results show that most pterosaurs are preserved predominantly through catastrophic events, often reflecting mass mortality episodes. By contrast, *Rhamphorhynchus* exhibits a uniquely attritional taphonomic signature, characterized by the gradual accumulation of individuals over time. These findings underpin a generalized catastrophic-attritional taphonomic (CATT) model, which provides a robust framework for reassessing the paleobiology of Solnhofen pterosaurs and other vertebrates from this iconic Lagerstätte.

RESULTS

Discovery and geological context

This study examines two of the smallest known specimens of *Pterodactylus antiquus*, MBH 250624-07 and SNSB-BSPG 1993 XVIII 1508 (Figure 1). Both specimens originate from the Upper Jurassic Solnhofen limestone deposits of Bavaria, southern Germany, dating to ~153–148 million years ago, spanning the upper Kimmeridgian to lower Tithonian stages. The first specimen, MBH 250624-07 (Figures 1A, 1B, and 1E), was collected from the lower Tithonian (Upper Jurassic) Altmühltal Formation (Malm Zeta 2) at Harthof near Eichstätt. The second specimen, SNSB-BSPG 1993 XVIII 1508 (Figures 1C, 1D, and 1F), was recovered from the older Torleite Formation (Malm Epsilon) of Brunn and is upper Kimmeridgian (Upper Jurassic) in age.[44]

Collectively referred to as the Solnhofen Archipelago, the Upper Jurassic platy limestones of the southern Franconian Alb represent a series of world-renowned Lagerstätten, celebrated for their exceptional fossil preservation. These deposits comprise a complex succession of lithological units formed within discrete carbonate basins, including the Altmühltal, Mörnsheim, Painten, and Torleite formations.[45]

Please cite this article in press as: Smyth et al., Fatal accidents in neonatal pterosaurs and selective sampling in the Solnhofen fossil assemblage, Current Biology (2025), https://doi.org/10.1016/j.cub.2025.08.006

During the Late Jurassic, this region formed part of a semi-tropical seascape characterized by coral-sponge reefs and sponge-microbialite mounds that separated restricted marine basins interspersed with small islands.[41] Within these basins, finely laminated micritic carbonate sediments were deposited under stratified water column conditions, reflecting varied local depositional environments and stratigraphic intervals.[40]

The platy limestones or ''Plattenkalks'' that formed within these basins comprise a substantial sequence of calcareous sediments that accumulated at variable rates.[45] A key feature of this succession is the recurrent alternation of two distinct lithologies: Flinz and Fäule (plural Flinze and Fäulen). The Flinze are thin, hard, and brittle beds composed predominantly of micritic carbonate, typically containing >97% calcium carbonate with only minor amounts of clay and quartz. Fäulen are softer, finely laminated layers that have lower calcium carbonate content (80%–90%) and a proportionately higher content of clay and organic matter.[40,41,46] Fäulen represent prolonged periods of extremely low sediment accumulation, whereas Flinze are interpreted as marking brief intervals of increased energy and greatly increased sedimentation within the basin.[40,41] The development of ideas to explain this variation and the fossil content dates back more than three centuries.[47] Several models have been proposed,[40,41] but there is now general agreement that the Flinze represent rapid sedimentation resulting from suspension flows of carbonate muds generated by severe storm events (tropical cyclones), while the Fäulen reflect much slower rates of ''normal'' background sedimentation.[40,41]

Much of the fossil content of the Solnhofen Archipelago is linked to storm events. The tetrapod assemblage is overwhelmingly dominated by aerial taxa. Approximately 65% of recorded tetrapod specimens are volant, with pterosaurs alone comprising around 63%, while marine tetrapods account for only 20.5% and terrestrial taxa just 14.5%.[42] Strong winds directly and disproportionately affected volant animals, including insects, pterosaurs, and basal avialans such as *Archaeopteryx*. Indirectly, storms caused mixing of surface waters with deeper hypersaline, oxygen-depleted bottom waters, leading to mass mortalities among marine invertebrates and fish. For creatures that sank to the seafloor, these hypersaline and oxygen-poor conditions greatly inhibited scavenging and decomposition, creating an ideal environment for the exceptional preservation of delicate skeletal elements and, in rare cases, soft tissues. Storm-generated mud rapidly buried these organisms, ensuring fossilization. As with most exceptionally preserved Solnhofen fossils, the specimens discussed here were recovered from the base of these storm deposits. See Viohl[40,41] and references therein for a detailed, integrative model incorporating climate, sedimentation, and taphonomy.

Taxonomy

Both MBH 250624-07 and SNSB-BSPG 1993 XVIII 1508 are assigned to *Pterodactylus antiquus* based on a unique combination of characters.[26] These include flat, conical teeth with crowns about twice as long as their basal width, extending to the jaw tip and decreasing in size posteriorly; a wing phalanx 2 length >90% of wing phalanx 1 length; a dorsally curving preacetabular process of the ilium; a metatarsal II that is longer than metatarsal I; a relatively short metatarsal IV (<85% the length of metatarsal I); and pedal phalanx III-1 and III-3 of subequal length.

Following taxonomic revision, *Pterodactylus antiquus* is now represented by nearly 50 individuals.[26] The smallest individuals, including MBH 250624-07 and SNSB-BSPG 1993 XVIII 1508, are nearly identical in size, with skull lengths of 25–33 mm, forelimb lengths of 85–105 mm, and estimated wingspans of 180–220 mm (Figures 1E, 1F, and 2A).

Ontogenetic status

It is generally accepted that the smallest individuals of *Pteordactylus* are osteologically immature, with several identified as neonates,[6,26,28] though these assignments remain untested. In that context, a growing body of literature has documented perinatal (late embryonic and neonatal) pterosaurs highlighting histological, osteological, and morphometric characteristics that distinguish them from later growth stages. Several well-preserved embryos have been shown to be near term,[48–50] comparable to neonates in all respects except for their containment within an egg.[28] These individuals enable confident assignment of ontogenetic status and provide valuable data on the development of perinatal individuals.

We used this data to conduct the first systematic assessment of the ontogenetic status of putative *Pterodactylus antiquus* neonates using 22 characters, each with three states reflecting different developmental stages. These characters were compiled from published works on pterosaur ontogeny.[1,20,21,27,28,48–61] Two near-term ornithocheirid embryos,[48,49] a near-term embryo and two neonates of *Pterodaustro guinazui*,[50,54] and five putative neonates together with three larger individuals of *Pterodactylus antiquus* were scored for each of the 22 osteological characters (Figure 2B; see STAR Methods).

As expected, developmental profiles for known embryos and neonates are marked by character states indicating absent or incomplete ossification of skeletal elements (e.g., carpals and tarsals), unfused epiphyses and diaphyses (e.g., wing phalanx 1 and proximal extensor tendon tubercle), and lack of co-ossification of discrete elements (e.g., maxilla and premaxilla). Putative neonates of *Pterodactylus antiquus* display remarkably similar profiles, closely matching those of the ornithocheirid embryos. In some respects, they appear even less developed than the *Pterodaustro* specimens, which show well-ossified limb bones, caudal vertebrae, and pedal digit IV phalanges, features that remain only partially or completely unossified in *Pterodactylus*.

The developmental profile for a slightly larger *Pterodactylus* specimen, TM 10341, shares eight character states with the putative neonates but exhibits more advanced development in eight others. Notably, the cranium, mandible, caudal series, carpals, and intermediate phalanges in pedal digit IV are fully ossified. Evidently, TM10341 represents a later, though still immature, stage of skeletal development. Two well-known examples of *Pterodactylus antiquus* (SNSB-BSPG 1937 I 18 and SNSB-BSPG AS I 739) with skull lengths three to four times the length of the skulls of the smallest individuals exhibit ossification states that are more derived than those of the putative neonates. Even so, these individuals retain several features, such as lack of fusion of the proximal tarsals to the tibia, that suggest that they had not reached full osteological maturity.

Please cite this article in press as: Smyth et al., Fatal accidents in neonatal pterosaurs and selective sampling in the Solnhofen fossil assemblage, Current Biology (2025), https://doi.org/10.1016/j.cub.2025.08.006

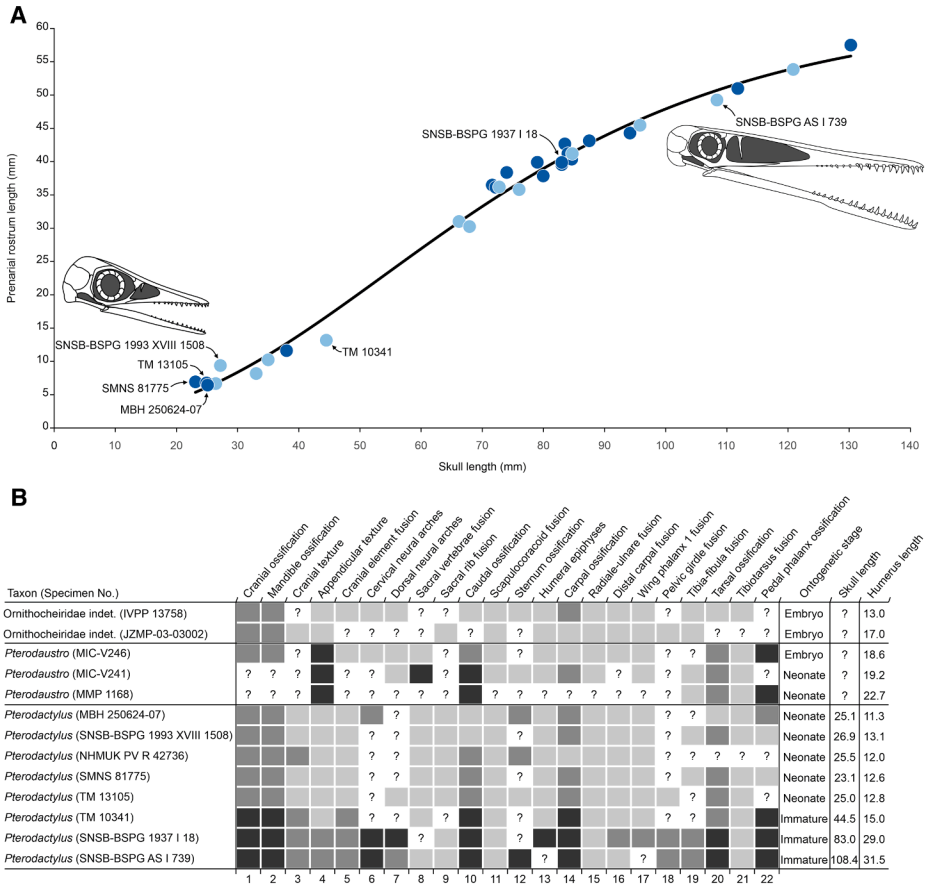

Figure 2. Ontogenetic variation in *Pterodactylus antiquus*

(A) Plot illustrating the relationship between skull length and prenarial rostrum length, demonstrating changes in cranial proportions throughout ontogeny along a logarithmic curve, from osteologically highly immature (neonates) to larger juvenile individuals. Due to extreme taphonomic bias, no complete skulls of mature individuals have been recovered. Each data point represents a single individual, and dark blue circles indicate specimens with preserved soft tissue, while light blue circles denote those without. The neonate skull is reconstructed from MBH 250624-07, and that of the larger juvenile individual is based on the *Pterodactylus antiquus* holotype, SNSB-BSPG AS I 739 (not to scale).

(B) Comparison of the osteological maturity of five putative neonates of *Pterodactylus antiquus* calibrated against embryos (Ornithocheiridae, *Pterodaustro*), neonates (*Pterodaustro*), and early immature and late immature examples of *Pterodactylus antiquus*. Variation in ornament for individual entries reflects three distinct levels of osteological maturity: light gray = skeletal elements poorly ossified or unossified, no fusion of epiphyses and diaphyses, no fusion of composite skeletal elements; mid gray = skeletal elements partly ossified, partial co-ossification of epiphyses and diaphyses, partial co-ossification of composite skeletal elements; dark gray = skeletal elements fully ossified, epiphyses and diaphyses fully co-ossified, composite skeletal elements fully co-ossified. Skull and humerus length in mm.

See also Data S1 for more details.

These developmental comparisons strongly support the hypothesis that the smallest individuals of *Pterodactylus antiquus* represent the neonatal growth stage. This conclusion is supported by the relative size distribution across the *P. antiquus* hypodigm. The largest examples (MBH 250624-10, MBH 250624-11) have an estimated skull length of 214–238 mm, eight times that of the smallest individuals (~25 mm). In MBH 250624-11, humerus length is 62 mm, over five times that of the smallest individual (MBH 250624-07: 11.3 mm). These proportions compare almost exactly to those for the hypodigm of *Pterodaustro guinazui*, where the largest relatively complete individual (MIC-V263) has a skull length eight times that of a hatchling (MIC-V246) and a humerus length 5.6 times that of the same hatchling.[54,56,60,62]

The precise age of the smallest *Pterodactylus* individuals is difficult to determine, but multiple lines of evidence (limited ossification, morphometric indices, and relative size) strongly support their identification as neonates with minimal post-hatching growth. That these individuals form a tight cluster defining the lower end of the size range in *P. antiquus* (Figure 2A) is also consistent with this idea and suggests that they represent hatchling size. Given that rapid postnatal growth is often assumed in pterosaurs[31] and supported by the fibrous texture of elongate cranial and appendicular bones, it is likely that their age at death would have been days or weeks, rather than months or years.

Skeletal trauma in *Pterodactylus antiquus*

MBH 250624-07 and SNSB-BSPG 1993 XVIII 1508 exhibit trauma to their humeri, characterized by complete oblique diaphyseal fractures (Figure 3). In MBH 250624-07, the fracture is located one-third of the way from the distal end of the left

Please cite this article in press as: Smyth et al., Fatal accidents in neonatal pterosaurs and selective sampling in the Solnhofen fossil assemblage, Current Biology (2025), https://doi.org/10.1016/j.cub.2025.08.006

CellPress
OPEN ACCESS

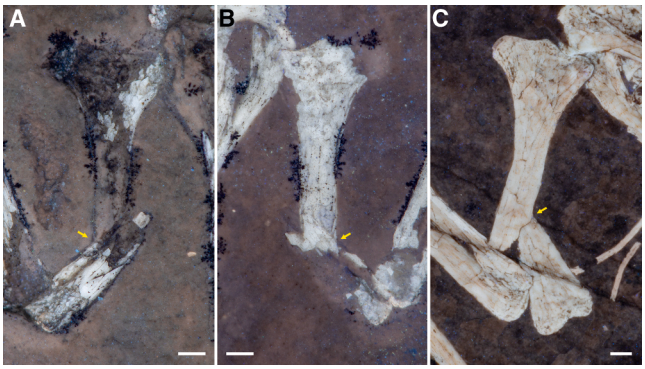

Figure 3. Comparison of oblique diaphyseal humeral fractures in *Pterodactylus antiquus*

(A and B) Part and counterpart of the left humerus from MBH 250624-07.
(C) Right humerus of SNSB-BSPG 1993 XVIII 1508 in ventral view exhibiting a similar fracture pattern.
Scale bars: 1 mm.

humerus and extends approximately 20% of the total bone length (Figures 3A and 3B). The fracture edges are sharp and clean, showing no signs of bone remodeling, and the distal portion of the humerus is displaced anteriorly, angled at approximately 40° relative to the proximal shaft.

SNSB-BSPG 1993 XVIII 1508 exhibits a strikingly similar complete, oblique diaphyseal fracture, affecting the right humerus (Figure 3C). This fracture is also located about one-third of the way from the distal end and extends between 20% and 25% of the total bone length, mirroring MBH 250624-07. The edges of the fracture in SNSB-BSPG 1993 XVIII 1508 are similarly sharp and clean, with no evidence of remodeling. Unlike MBH 250624-07, the distal section of the humerus is displaced posteriorly yet shares an angle of approximately 40° relative to the respective proximal shaft.

These fractures represent pre-fossilization breaks and do not reflect common post-depositional damage to Solnhofen fossils. Compaction deformation typically produces longitudinal buckling of bones, and splitting of fossil bones during extraction usually results in clearly demarcated breaks aligned with bedding planes.[4,37] Neither process can produce the observed rotational displacement of bone fragments, which must have occurred prior to burial.

Quantitative taphonomic analysis

Data on skeletal completeness, articulation, and soft tissue preservation for 42 specimens of *Pterodactylus antiquus*—ranging from highly immature to skeletally mature (skull length 23–236 mm) (Figures 4A–4C)—plotted against a size proxy, reveal two distinct taphonomic pathways. Most specimens, including MBH 250624-07 and SNSB-BSPG 1993 XVIII 1508, are small to medium-sized, with high degrees of completeness and articulation (Figures 4A–4C and 5A–5C), and often exhibit soft tissue preservation.

By contrast, remains of larger *Pterodactylus antiquus* are much rarer in the Solnhofen Archipelago (Figure 4A), are often found as incomplete and disarticulated elements (Figures 4B, 4C, and 5D–5F), and lack accompanying fossilized soft tissues.

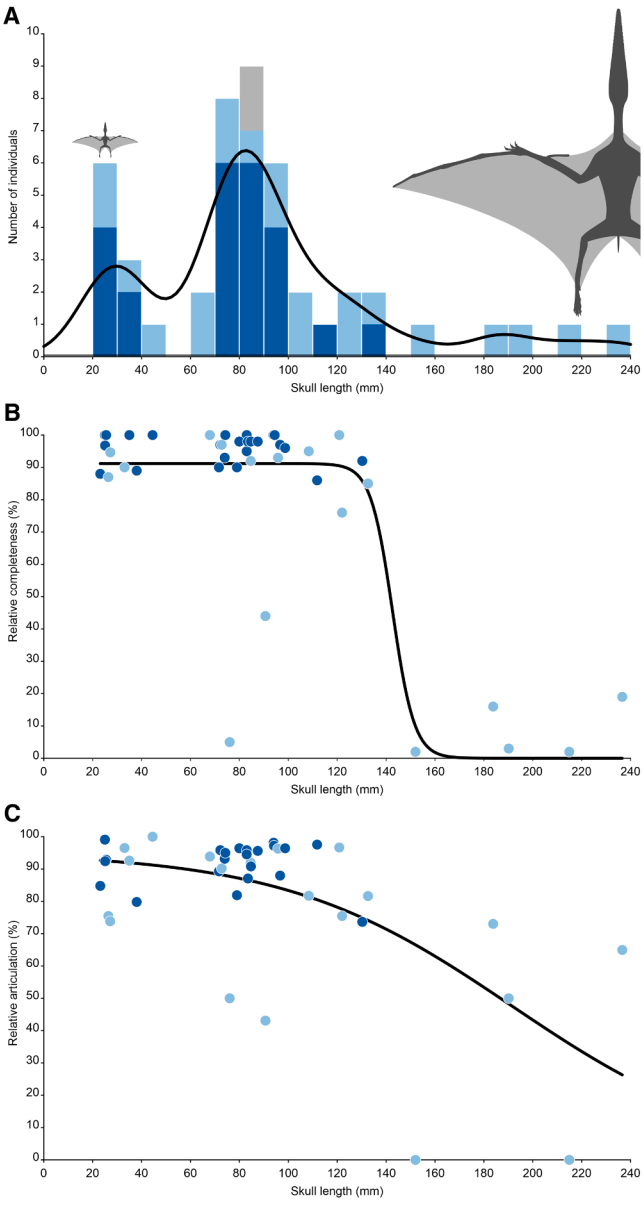

Figure 4. Taphonomic profile of *Pterodactylus antiquus* in the Solnhofen assemblage

(A) Size-frequency histogram illustrating a catastrophic mortality profile with kernel density estimate, primarily comprised of neonate and osteologically immature individuals. Silhouettes highlight the size disparity between the smallest and largest known specimens.
(B) Scatterplot depicting the relationship between body size (using skull length as a proxy) and relative completeness, revealing a nearly bimodal distribution. Individuals with skull lengths < 140 mm exhibit high completeness, while those with skull lengths > 140 mm show significantly lower completeness.
(C) Scatterplot illustrating the relationship between body size (using skull length as a proxy) and relative articulation, demonstrating a similar but more gradual decline in articulation as body size increases. Dark blue circles represent specimens with preserved soft tissue, and light blue circles indicate those without. Gray denotes lost specimens where the presence or absence of soft tissue could not be determined.
See also Figure S1 and Data S1 for more details.

Please cite this article in press as: Smyth et al., Fatal accidents in neonatal pterosaurs and selective sampling in the Solnhofen fossil assemblage, Current Biology (2025), https://doi.org/10.1016/j.cub.2025.08.006

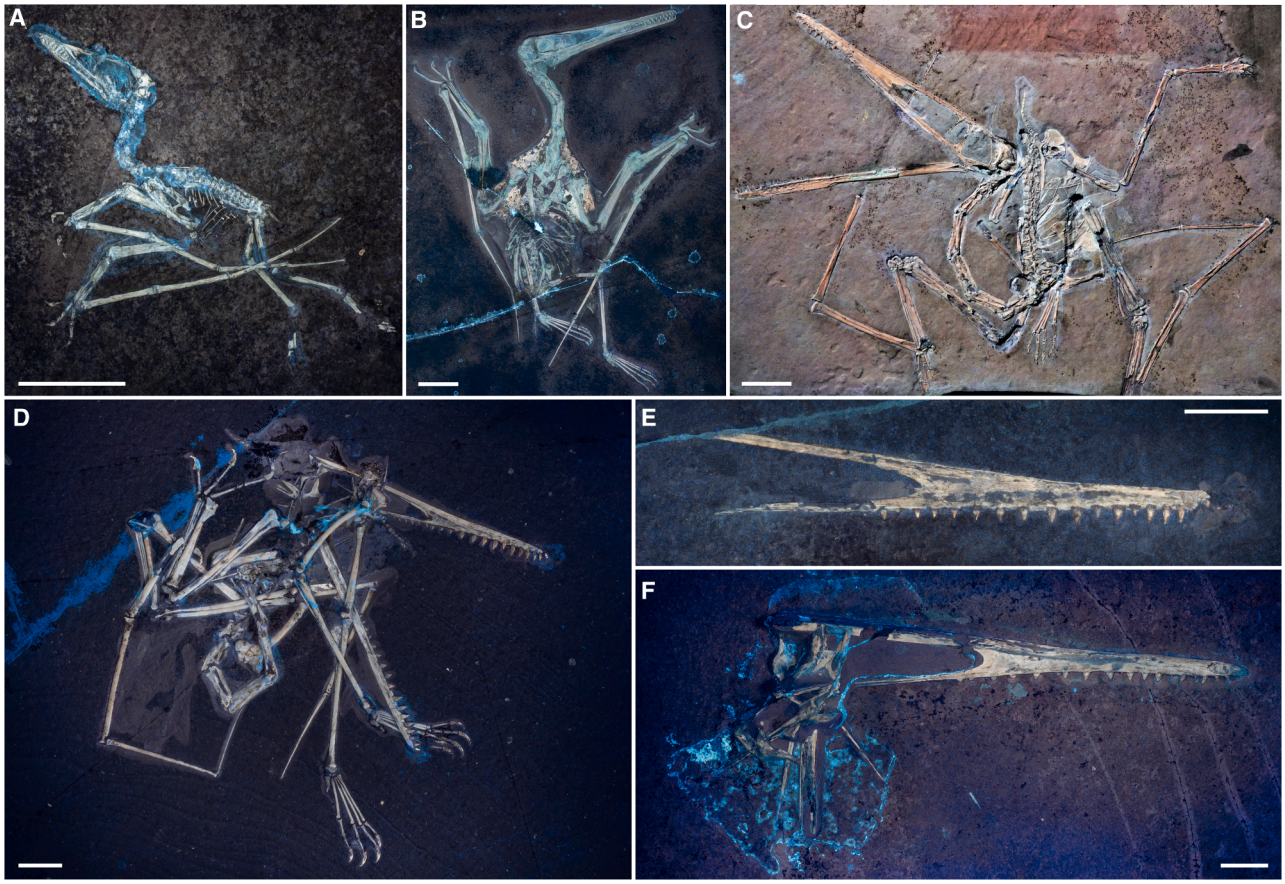

Figure 5. Examples of different taphonomic classes in *Pterodactylus antiquus* photographed under UV light

(A–C) Complete, well-articulated, immature individuals. (A) Complete and well-articulated but osteologically highly immature skeleton of a neonate, TM 13105, preserved in a lateral recumbent posture, and associated with soft tissue preservation. (B) Exceptionally preserved example of an osteologically immature individual, SNSB-BSPG 1937 I 18, in a spread-eagle posture, with extensive soft tissue. Unfortunately, much of this was likely removed during preparation. (C) Complete and relatively well-articulated but osteologically immature specimen, SNSB-BSPG AS I 739 (holotype), preserved in a sprawled, spread-eagle posture with an opisthotonic neck posture; no evidence of soft tissue preservation. Image courtesy of Helmut Tischlinger.

(D) Relatively large individual, Bürgermeister-Müller-Museum, Solnhofen (BMMS) uncat, with a near-complete but somewhat disarticulated skeleton showing a high degree of osteological maturity.

(E and F) Fragmentary remains of the largest known individuals. (E) Isolated rostrum from a large individual, MBH 250624-09. (F) Disarticulated cranium of an exceptionally large individual, MBH 250624-10, that, nevertheless, shows some evidence of osteological immaturity.

Scale bars: 20 mm.

To compare patterns in *Pterodactylus* with other Solnhofen pterosaurs, we analyzed additional well-sampled taxa using established preservation categories: complete articulated skeletons (type 1), partially disarticulated but life-like arrangements (type 2a), scattered elements across the deposit (type 2b), and isolated regions of the skeleton (type 3).[1]

No other pterodactyloid from the Solnhofen assemblage approaches the abundance of *Pterodactylus antiquus* (Figure 6A). Most other taxa are represented by relatively few specimens mired in poorly resolved taxonomies that preclude the construction of species-level comparative taphonomic profiles. However, when members of the pterodactyloid clade Ctenochasmatoidea (e.g., *Ctenochasma elegans*, *Aurorazhdarcho micronyx*, and *Ardeadactylus longicollum*) are considered collectively (n = 56), they plot in a pattern similar to that observed in *P. antiquus* (Figure 6B). The ctenochasmatoid sample shows a pronounced negative size bias. Skeletal completeness and articulation are also highly skewed according to body size. Among smaller individuals with skull lengths <100 mm, 66.7% are fully articulated, while 33.3% show some degree of disarticulation. By contrast, larger individuals with skull lengths >100 mm are far less intact, with only 6.9% being well-articulated, 27.6% partially to fully disarticulated, and 65.5% represented solely by isolated body segments. Among the isolated ctenochasmatoid body segments, skull and forelimb elements are equally represented (each comprising 42.1%), followed by hindlimbs (26.3%). This combination of a catastrophic L-shaped mortality profile and the preferential preservation of smaller individuals indicates that the same mechanisms were responsible for sampling other pterodactyloids in the Solnhofen assemblage, not just *P. antiquus*.

A very different taphonomic profile was recovered for the non-pterodactyloid *Rhamphorhynchus muensteri*, the most abundantly represented pterosaur in the Solnhofen assemblage,

Please cite this article in press as: Smyth et al., Fatal accidents in neonatal pterosaurs and selective sampling in the Solnhofen fossil assemblage, Current Biology (2025), https://doi.org/10.1016/j.cub.2025.08.006

CellPress
OPEN ACCESS

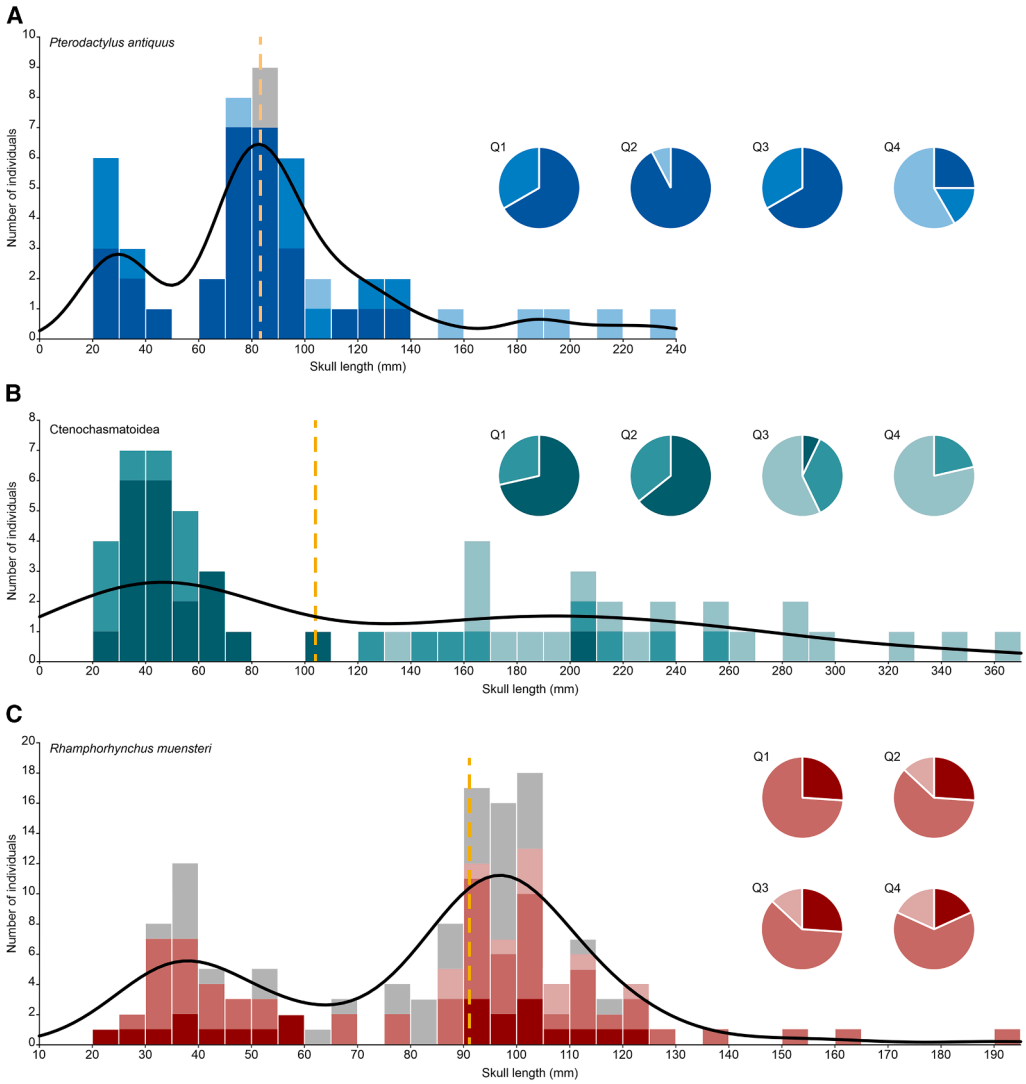

Figure 6. Comparison of the taphonomic profile of *Pterodactylus antiquus* with other Solnhofen pterosaurs

Size-frequency histograms illustrate the abundance and preservational modes across size classes (using skull length as a proxy) for (A) *Pterodactylus antiquus*; (B) Ctenochasmatoidea (including *Ardeadactylus*, *Aurorazhdarcho*, *Ctenochasma*, *Cycnorhamphus*, *Gnathosaurus*, and *Petrodactyle*, as well as indeterminate ctenochasmatoid material); and (C) *Rhamphorhynchus muensteri*. Preservational modes are indicated by dark tones for fully articulated skeletons, mid-tones for partially to fully disarticulated skeletons, light tones for isolated skeletal elements, and gray for unknown modes. The dashed line denotes the median. Pie charts depict the relative abundance of known preservation modes within each quartile of the size distribution. Pterodactyloids (A) and (B) display L-shaped catastrophic mortality profiles dominated by neonatal and immature individuals. These relatively small individuals exhibit more complete preservation than larger size classes, which are predominantly represented by fragmentary remains. *Rhamphorhynchus* (C) exhibits a U-shaped attritional mortality profile with a slight bias toward relatively large individuals. Preservation modes, dominated by partially disarticulated skeletons, are consistent across size classes.
See also Figures S1–S3 and Data S1 for more details.

known from over 130 individuals.[17] Unlike pterodactyloids, the taphonomic profile of *Rhamphorhynchus* is left-skewed, with the most abundant size classes occurring in the right half of the distribution, typical of an attritional, U-shaped mortality profile (Figure 6C).[63]

Preservational modes in *Rhamphorhynchus* differ from those of pterodactyloids, with both small and large individuals showing similar patterns. Fully articulated remains are rare in both smaller (skull lengths <91.1 mm; 27.3%) and larger individuals (skull lengths >91.1 mm; 21.3%), and fragmentary remains are also uncommon in these size groups (6.8% and 17.0%, respectively). Partially to fully disarticulated skeletons are most common, comprising 65.9% of smaller and 61.7% of larger specimens (Figure 6C).

The positive size bias and dominance of somewhat disarticulated remains across all size classes of *Rhamphorhynchus* are inconsistent with the patterns observed in other Solnhofen pterosaurs. Uniquely for Solnhofen pterosaurs, the *Rhamphorhynchus* record is dominated by attritional rather than catastrophic sampling.

Please cite this article in press as: Smyth et al., Fatal accidents in neonatal pterosaurs and selective sampling in the Solnhofen fossil assemblage, Current Biology (2025), https://doi.org/10.1016/j.cub.2025.08.006

DISCUSSION

Wing fracture etiology

Traumatic injury to the forelimbs is among the most prevalent skeletal pathology in volant vertebrates. Post-fledgling birds and bats frequently exhibit fractures to the bones of the wing, reflecting the inherent risks associated with powered flight.[64,65] These injuries in extant flying animals provide a useful comparative framework for interpreting similar forelimb pathologies in pterosaurs.

Despite differences in wing structure, the humerus in birds, bats, and pterosaurs shows notable convergence in form and function.[66] The humerus anchors the wing to the body, serving as the principal element for transmitting aerodynamic loads and muscular forces during flight. Subjected to high torsional and bending stresses, the humerus is often the most structurally reinforced element in the forelimb skeleton of birds, bats, and pterosaurs.[67] In extant birds, it is optimized to resist torsional loads more effectively than transverse bending misaligned with its principal load-bearing axis.[68] This predisposes the humerus to specific failure modes, particularly under unusual or extreme conditions.

Oblique diaphyseal fractures of the humerus, produced by indirect, often rotational or angular forces, are among the most commonly observed skeletal injuries in birds.[65,69] These injuries typically result from abrupt, non-impact trauma that acts at a distance from the fracture site, rather than direct impact with an object.[70] Strikingly similar oblique humeral fractures are present in the pterosaur specimens MBH 250624-07 and SNSB-BSPG 1993 XVIII 1508, both of which exhibit pronounced displacement of the distal humeral fragment. This pronounced movement results from the abrupt release of tension exerted by surrounding muscles and tendons, particularly the flexors and extensors acting across the elbow joint, at the point of fracture; this can cause rotational and shearing forces that exacerbate fragment misalignment.[68,71,72]

Three lines of evidence strongly suggest that the trauma was perimortem. Firstly, there is no osteological evidence for healing, such as periosteal or endosteal proliferation. In birds, initial healing responses are histologically visible within 5 days post-injury,[73] and within 3 weeks in reptiles such as lizards.[74] Secondly, the observed *in vivo*-style association and displacement of bone fragments, attributable to muscle tension, indicates that the fractures and subsequent burial occurred while the soft tissues remained intact and the musculature was still capable of exerting mechanical forces on the humerus. Thirdly, fresh breaks typically exhibit oblique angles and smooth edges, reflecting the bone's elasticity at the time of injury. Dry breaks, which occur after the bone has dried out, are more often transverse with rough, jagged edges.[75]

The single oblique fracture with its smooth breakage plane is inconsistent with damage from scavenging or predation, which typically results in multiple injuries, including irregular or crenulated fractures, punctures, or gnaw marks.[76] The absence of these features, combined with the well-preserved articulation of the skeleton, strongly argues against either cause.

What scenario could produce such acute, catastrophic loading of the wing in the brief interval prior to burial within storm-generated Flinze? The sedimentological,[77] taphonomic,[40,41,78] and paleoenvironmental evidence[39–41] associated with both specimens collectively points to a plausible explanation. The same storm events responsible for the burial of these individuals also transported the pterosaurs into the lagoonal basins and were likely the primary cause of their injury and death.

Storms generate hazardous environmental conditions, characterized by violent gusts, turbulent airflows, extreme wind shear, and powerful wave action. The impact of any of these phenomena on the pterosaur wing can be simply modeled as a dynamic moment load acting through the wing's centroid (its geometric center).

Transmission of these loads to the body can be represented by modeling the wing spar (forelimb) as a beam attached at one end to the body via the shoulder joint. The load experienced by each bone comprising the wing spar is directly related to its distance from the wing's centroid. According to the principle of moments, the greatest loads would be borne by the element closest to the point of attachment (i.e., the humerus).

This also applies during normal flight, with biomechanical analyses finding that the humerus of flying vertebrates bears most of the stresses imposed on the wing.[79] Although structurally robust, the humerus is particularly vulnerable to fractures resulting from torsional forces, which produce high shear strains within the bone.[80] Its greatest risk of failure arises under sudden, atypical loading of the wing surface that pushes these strains beyond its torsional capacity.[80]

Evidence from mass mortality of extant birds and bats during severe storms supports this interpretation.[81,82] Single events can cause the deaths of up to hundreds of thousands of individuals.[81,83,84] Such storms are known to cause traumatic injuries, with injury patterns differing between terrestrial and marine settings. Terrestrial storm fatalities commonly show a high incidence of multiple skeletal fractures to the skull, neck, and body, caused by collisions with the ground or other solid objects,[85,86] a pattern inconsistent with infrequent and isolated fractures in Solnhofen pterosaurs. By contrast, marine storm fatalities tend to exhibit rare, isolated fractures to the wings,[87,88] often as a result of wind and wave action,[83,89] which better match the injuries observed in these pterosaurs. Reports of wing fractures in a small percentage of avian storm victims are widely reported, but detailed records of fracture location and nature are absent from the literature. Most storm-killed birds show no skeletal trauma, with death resulting from other causes, including exhaustion and drowning.[81,83] Storms also disproportionately affect smaller birds, poor fliers, and juveniles, who are vulnerable due to their lower load-bearing capacities and inexperience in the air.[81,83,84] In combination with sedimentological and paleoenvironmental data, the taphonomic profile of *Pterodactylus* in the Solnhofen assemblage, consisting mainly of juveniles with most individuals showing no skeletal trauma but rare cases of wing fractures, is entirely consistent with storm-related mortality in a marine setting.

CATT model

We propose the following sequence of events (Figure 7), formally termed the CATT model. (1) MBH 250624-07 and SNSB-BSPG 1993 XVIII 1508 were caught in storms while flying over or driven out over the Solnhofen lagoon by storm conditions. (2) Powerful gusts of wind or impact with the water surface produced

Please cite this article in press as: Smyth et al., Fatal accidents in neonatal pterosaurs and selective sampling in the Solnhofen fossil assemblage, Current Biology (2025), https://doi.org/10.1016/j.cub.2025.08.006

CellPress
OPEN ACCESS

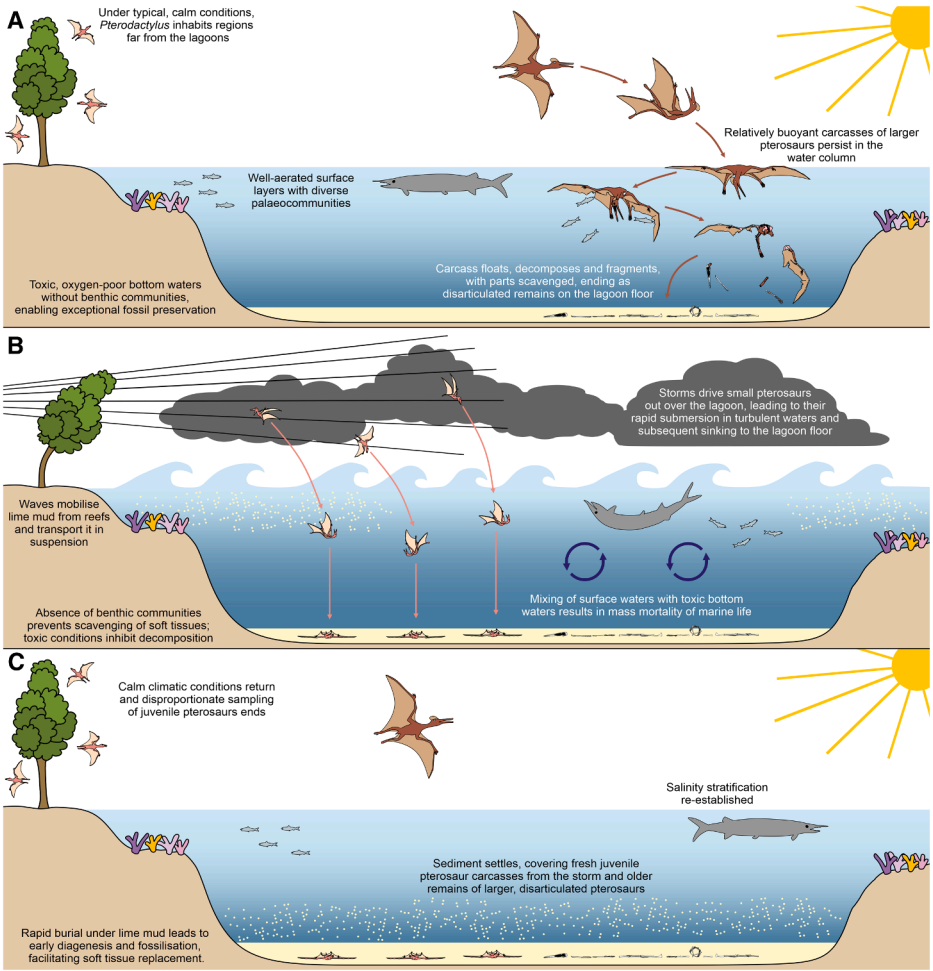

Figure 7. The bimodal CATT model illustrating catastrophic and attritional taphonomic pathways

(A) Under typical conditions, preservation of pterosaurs is rare. Only disarticulated or fragmentary remains of larger individuals occasionally reach the lagoon floor, while smaller pterosaurs are largely excluded from this pathway.

(B) Storm events disproportionately affect small, immature pterodactyloids. Turbulent seas rapidly submerge carcasses, while mixing of toxic bottom waters with surface waters leads to mass mortality of marine life. These conditions inhibit scavenging and decomposition, allowing pterosaur carcasses to settle intact on the lagoon floor.

(C) Lime mud transported by storms rapidly buries the remains, initiating fossilization. This burial promotes exceptional preservation of soft tissues and captures fragmentary remains of larger individuals deposited earlier.

Modified from Barthel[38] and Frey and Martill.[91]

See also Data S1 for more details.

torsional and bending forces that exceeded the humerus' load tolerance, resulting in an oblique fracture. (3) In either scenario, the injury would have rendered the pterosaur incapable of sustained flight, as even minor humeral rotational deformity severely impairs flight ability,[68] causing it to fall or remain stranded on the water. (4) Storm-driven waves and surface turbulence likely led to drowning and waterlogging. Inhaled water filled the lungs, displacing air and sharply reducing buoyancy, which allowed otherwise buoyant animals to sink rapidly to the lagoon floor (Figure 7B).[90] (5) The carcass was then swiftly buried by fine-grained carbonate muds deposited by the storm,[40,41,78] facilitating fossilization (Figure 7C).

This catastrophic taphonomic pathway, triggered by storm events, was likely the principal mechanism by which small- to medium-sized pterodactyloids (skull length <140 mm; Figure 4) entered the Solnhofen assemblage. Unhealed, fractured wing phalanges observed in immature specimens of other taxa, *Diopecephalus kochi* (SMF R 4072) and *Ctenochasma elegans* (PMZ A/III 1000),[1] are consistent with perimortem catastrophic wing failure. As mentioned above, skeletal trauma in marine storm mortality events is uncommon. These individuals likely represent only the most visible examples of storm-related mortality in the fossil record. It is probable that many other Solnhofen pterosaurs died during storms, but causes such as wing membrane damage, exhaustion, or drowning have left no trace in the fossil record. Experimental work has shown that drowning is the most viable explanation for how small, lightweight flying animals can become sufficiently dense to sink to the lagoon floor.[90] Hypersaline, anoxic bottom waters, combined with rapid burial by storm-driven carbonate muds, suppressed decay and prevented the

Please cite this article in press as: Smyth et al., Fatal accidents in neonatal pterosaurs and selective sampling in the Solnhofen fossil assemblage, Current Biology (2025), https://doi.org/10.1016/j.cub.2025.08.006

buildup of gases that would otherwise cause carcasses to bloat and float after an initial period on the seafloor.

By contrast, remains of larger pterodactyloids (skull length >140 mm) are relatively rare, consistently incomplete, and partially disarticulated (Figures 4, 5E, and 5F). These specimens appear to have entered the fossil record through an alternative, attritional taphonomic pathway characterized by prolonged surface exposure and floating, followed by gradual disintegration on the lagoon floor (Figure 7A).[1,91] The skeletons of small individuals were composed of relatively solid elements with thick bone walls and little or no central cavity (Figures 1A–1D). By contrast, limb bones in large individuals have large central cavities and relatively slender walls, a pattern observed in other pterosaurs, including *Rhamphorhynchus*[27] and *Pterodaustro*,[56] with, in the case of *Pterodactylus*, pneumatization extending into the cervical series. This rendered large individuals relatively more buoyant and less likely to sink quickly than smaller individuals, further biasing patterns of preservation.

Since all specimens were ultimately buried by storm-generated sedimentation, the degree of skeletal completeness and articulation reflects the interval between death and burial. The well-articulated, largely intact preservation of smaller individuals suggests that death occurred shortly before, or more likely during, the storm events that led to burial, with no more than a few hours to days elapsing between death and final entombment.[92] The fragmentary remains of larger specimens suggest a longer postmortem interval with greater decay, transport, and disarticulation. Assuming avian-type decay rates and patterns, at least 4 days would be required for skull separation and 12 days or more for detachment of limbs from the body.[93] After this initial period in a typical decay environment, the remains settled for an unknown duration in the reduced-decay conditions of the lagoon floor before final entombment during subsequent storm events.[42,78]

The widespread presence of catastrophic L-shaped pterodactyloid mortality profiles (Figures 6A and 6B), preferential preservation of smaller individuals, and rare wing fractures across multiple taxa indicate that storm events were the primary mechanism sampling other pterodactyloids in the Solnhofen assemblage.

Storm-related transport and burial likely also explain the presence of several rare, exceptionally preserved non-pterodactyloid taxa in the assemblage (including *Anurognathus*, *Scaphognathus*, and *Propterodactylus*), which were occasionally carried from more distant habitats into the lagoons and rapidly buried in the Flinze.

However, it does not account for the left-skewed, attritional taphonomic profile of the highly abundant *Rhamphorhynchus*. The positive size bias and predominance of somewhat disarticulated remains across all size classes of *Rhamphorhynchus* are inconsistent with rapid burial during storm events. This is further supported by the near absence of perimortem pathologies despite the large sample size. Additionally, the apparent rarity of fragmentary remains, even among larger individuals, suggests minimal carcass transport. Together, these patterns indicate that, unlike other pterosaurs in the Solnhofen assemblage, which appear to have been sampled as part of rare events that brought allochthonous taxa into the lagoonal basins, *Rhamphorhynchus* was an autochthonous component of the basin ecosystems, consistent with interpretations based on its functional morphology.[5–7]

Implications for precocial flight ability in pterosaurs

An important consequence of the storm-modulated catastrophic taphonomic pathway is that, among non-marine animals, it disproportionately sampled aerial vertebrates (pterosaurs, basal avialans) and invertebrates (winged insects).[4,37,42] This is of particular significance in the case of MBH 250624-07 and SNSB-BSPG 1993 XVIII 1508, whose skeletal features indicate a neonatal ontogenetic stage (see above). It has been argued that pterosaurs had a precocial ability, taking flight at a very early age.[6,28,29] While this hypothesis has been challenged,[27,30,31] it is supported by multiple lines of evidence, including patterns of ossification, skeletal proportions, and evidence of wing membranes in several of the smallest known individuals of *Pterodactylus antiquus*, including MBH 250624-07, NHMUK PV R 42736, and TM13105 that, in terms of their extent and structure, match those of somewhat larger individuals such as BSPG-SNSB 1937 I 18 (Figure 5B) and NHMW 1975/1756. Collectively, these structures form a fully developed flight apparatus that, according to aerodynamic analyses,[29] generated sufficient force to enable active flight. While compelling, these lines of evidence remain circumstantial. However, the discovery of two individuals with perimortem wing pathologies characteristic of flight-related injuries (distinct from those typically sustained by altricial birds[94]), preserved in a marine deposit, provides direct evidence that these neonates were capable of flight. Four other neonates (NHMUK PV R 42736, NHMUK PV R388, SMNS 81755, and TM13105), closely comparable in size and ontogenetic status to MBH 250624-07 and SNSB-BSPG 1993 XVIII 1508 (see above), lack skeletal trauma but likely perished in storms and provide additional evidence of precocial flight ability.

Implications for pterosaur paleoecology and evolution

Reference is often made to the "Solnhofen pterosaur fauna,"[21,22,95] and it could imply that the Solnhofen Archipelago represents a single, unified ecosystem in which all known pterosaur species coexisted. This is incorrect. *Rhamphorhynchus muensteri*, by far the most abundantly represented pterosaur in the Solnhofen deposits,[17] appears to have been an autochthonous component of the local ecosystem and likely inhabited the lagoons and reefs of the Solnhofen region. By contrast, other, less abundant species such as *Pterodactylus antiquus*, *Diopecephalus kochi*, *Ctenochasma elegans*, *Aurorazhdarcho micronyx*, and extreme rarities including *Anurognathus ammoni*, *Scaphognathus crassirostris*, *Altmuehlopterus rhamphastinus*, and *Germanodactylus cristatus* most likely represent accidental allochthonous elements that inhabited more distant regions of the archipelago or beyond but were transported into the Solnhofen lagoons as a result of the tropical storms, the primary mechanism that generated this fossil Lagerstatte.[4] Such biases likely extend to other groups of non-marine tetrapods preserved in the Solnhofen assemblage, representatives of which are all relatively small-bodied.[4]

Our results underscore profound preservational biases in the Solnhofen pterosaur assemblage. Small individuals are overrepresented, while larger, mature pterosaurs are largely absent from the fossil record. The CATT model explains the

preponderance of small individuals but also emphasizes the rarity of larger individuals, attributable to the much longer periods of time between death and final burial, during which scavenging and decay likely removed most carcasses from the taphonomic pathway. Taphonomic profiles for other pterosaur Lagerstätten, such as the Lower Jurassic Posidonia Shales of southern Germany,[96,97] the Lower Cretaceous Crato and Romualdo Formations of Brazil,[98,99] and the Upper Cretaceous Niobrara Chalk of the USA,[53] show almost the opposite pattern, dominated by relatively large semi-mature or mature individuals to the exclusion of small immature individuals. This almost certainly reflects the operation of fundamentally different taphonomic pathways from those shaping the Solnhofen pterosaur assemblage.

These biases have important implications for interpreting pterosaur paleoecology and evolution. The rarity of individuals exceeding two meters in wingspan in the Solnhofen Archipelago is evidently a taphonomic artifact, not a faithful record of size distribution in the Late Jurassic. This conclusion is supported by multiple discoveries of large pterosaurs from contemporaneous Upper Jurassic strata elsewhere.[100] As such, the Solnhofen assemblage is a poor proxy for determining overall pterosaur body size ranges during this interval.

More broadly, the pterosaur fossil record is exceptionally shaped by the Lagerstätten effect[101,102] more so than many other vertebrate clades, due to the rarity of depositional environments capable of preserving them. As a result, assemblages such as Solnhofen exert a disproportionate influence on our understanding of pterosaur evolution, despite being highly selective snapshots filtered by unique taphonomic and environmental conditions. It is entirely reasonable to acknowledge that the sum of all known pterosaur fossils remains insufficient to answer many of our most fundamental questions. The fossil record was not assembled for our benefit. Interpretations drawn from it must therefore be made cautiously, especially when comparing assemblages shaped by differing preservational pathways, lest we mistake artifacts of preservation for genuine evolutionary signals.

RESOURCE AVAILABILITY

Lead contact

Requests for further resources should be directed to and will be fulfilled by the lead contact, Robert Smyth (rabsmythpalaeo@gmail.com).

Materials availability

This study did not generate new, unique reagents.

Data and code availability

- New specimens reported in this study are held within publicly accessible collections: Museum Bergér, Harthof (MBH), and the Bavarian State Collection for Palaeontology and Geology, Munich (SNSB-BSPG). Original datasets necessary to replicate the results of this study are included in Data S1.
- This paper does not report original code.
- Any additional information required to reanalyze the data reported in this paper is available from the lead contact upon request.

ACKNOWLEDGMENTS

We are grateful to Oliver Rauhut and Markus Moser (Bavarian State Collection for Paleontology and Geology, Munich, Germany), Valentina Rosina and the late Martin Röper (Bürgermeister-Müller-Museum, Solnhofen, Germany), Christina Ifrim and Andreas Hecker (Jura-Museum, Eichstätt, Germany), Georg Bergér (Museum Bergér, Harthof, Eichstätt, Germany), Mike Day (Natural History Museum, South Kensington, UK), Julien Kimmig and Jannik Weidtke (Staatliches Museum für Naturkunde, Karlsruhe, Germany), Erin Maxwell and Rainer Schoch (State Museum of Natural History, Stuttgart, Germany), Jiang Shunxing and Wang Xiaolin (Institute for Vertebrate Paleontology and Paleoanthropology, Beijing, China), and Anne Schulp and Tim de Zeeuw (Teylers Museum, Amsterdam, the Netherlands) for facilitating access to specimens in their collections. We thank Benjamin Kear (Museum of Evolution, Uppsala University), Daniela Schwarz (Museum für Naturkunde, Berlin), Bruce Lauer (Lauer Foundation), Levi Shinkle (Wyoming Dinosaur Center), and Helmut Tischlinger for generously providing images of pterosaur specimens. R.S.H.S. and R.B. were supported by NERC studentships awarded through the Central England NERC Training Alliance (CENTA; grant reference NE/S007350/1) and the University of Leicester. D.M.U. acknowledges financial support from the University of Leicester and the John Templeton Foundation (grant ID 61408). Our thanks also go to Susan Beardmore, Roy Smith, and an anonymous reviewer for their insightful and constructive feedback. Additionally, we appreciate the support and guidance of editor Florian Maderspacher throughout the publication process.

AUTHOR CONTRIBUTIONS

Conceptualization, R.S.H.S. and D.M.U.; methodology, R.S.H.S., R.B., and D.M.U.; investigation, R.S.H.S., R.B., R.T., and D.M.U.; formal analysis and data curation, R.S.H.S., R.T., R.B., and D.M.U.; visualization, R.S.H.S.; supervision, D.M.U.; writing – original draft, R.S.H.S., R.B., R.T., and D.M.U.; writing – review and editing, R.S.H.S., R.B., R.T., and D.M.U.; and funding acquisition, R.S.H.S., R.B., and D.M.U.

DECLARATION OF INTERESTS

The authors declare no competing interests.

STAR★METHODS

Detailed methods are provided in the online version of this paper and include the following:

- KEY RESOURCES TABLE
- EXPERIMENTAL MODEL AND SUBJECT DETAILS
- METHOD DETAILS
  - Data Collection
- QUANTIFICATION AND STATISTICAL ANALYSIS
  - Body size estimates
  - Ontogenetic assessment
  - Quantitative taphonomy
  - Individual joints
  - Grouped joints
  - Taxonomic assignment of incomplete specimens: MBH 250624-09, MBH 250624-10, MBH 250624-11, MBH 250624-12, LF 2314P/LF 3398N

SUPPLEMENTAL INFORMATION

Supplemental information can be found online at https://doi.org/10.1016/j.cub.2025.08.006.

Received: May 14, 2025
Revised: July 15, 2025
Accepted: August 6, 2025

REFERENCES

1. Wellnhofer, P. (1970). Die Pterodactyloidea (Pterosauria) der Oberjura-Plattenkalke Süddeutschlands. Bayer. Akad. Wissenschaften Math. Naturwiss. Kl. Abh. *141*, 1–133.

2. Wellnhofer, P. (1975). Die Rhamphorhynchoidea (Pterosauria) der Oberjura-Plattenkalke Süddeutschlands, II. Systematische Beschreibung. Palaeontogr. A *148*, 132–186.
3. Barrett, P.M., Butler, R.J., Edwards, N.P., and Milner, A.R. (2008). Pterosaur distribution in time and space: an atlas. Zitteliana *B 28*, 61–107.
4. Arratia, G., Schultze, H.-P., Tischlinger, H., and Viohl, G. (2015). Solnhofen – Ein Fenster in die Jurazeit (Verlag Dr. Friedrich Pfeil).
5. Wellnhofer, P. (1991). The Illustrated Encyclopedia of Pterosaurs (Salamander Books).
6. Unwin, D.M. (2005). The Pterosaurs from Deep Time (Pi Press).
7. Witton, M.P. (2013). Pterosaurs: Natural History, Evolution, Anatomy (Princeton University Press). https://doi.org/10.1515/9781400847655.
8. Döderlein, L. (1929). Ein Pterodactylus mit Kehlsack und Schwimmhaut. Sitzungsber. Bayer. Akad. Wissenschaften Math. Naturwiss. Abt. *1929*, 65–76.
9. Broili, F. (1938). Beobachtungen an *Pterodactylus*. Sitzungsber. Bayer. Akad. Wissenschaften Math. Naturwiss. Abt. *1938*, 139–154.
10. Döderlein, L. (1929). Über *Rhamphorhynchus* und sein Schwanzsegel. Sitzungsber. Bayer. Akad. Wissenschaften Math. Naturwiss. Abt. *1929*, 1–46.
11. Wellnhofer, P. (1987). Die Flughaut von *Pterodactylus* (Reptilia, Pterosauria) am Beispiel des Wiener Exemplares von *Pterodactylus kochi* (Wagner). Ann. Naturhistorischen Museums Wien *88a*, 149–162.
12. Padian, K., and Rayner, J.M.V. (1993). The wings of pterosaurs. Am. J. Sci. *293*, 91–166. https://doi.org/10.2475/ajs.293.A.91.
13. Bennett, S.C. (2000). Pterosaur flight: the role of actinofibrils in wing function. Hist. Biol. *14*, 255–284. https://doi.org/10.1080/10292380009380572.
14. Bennett, S.C. (2016). New interpretation of the wings of the pterosaur *Rhamphorhynchus muensteri* based on the Zittel and Marsh specimens. J. Paleontol. *89*, 845–869.
15. Pittman, M., Barlow, L.A., Kaye, T.G., and Habib, M.B. (2021). Pterosaurs evolved a muscular wing–body junction providing multifaceted flight performance benefits: Advanced aerodynamic smoothing, sophisticated wing root control, and wing force generation. Proc. Natl. Acad. Sci. USA *118*, e2107631118. https://doi.org/10.1073/pnas.2107631118.
16. Frey, E., Tischlinger, H., Buchy, M.-C., and Martill, D.M. (2003). New specimens of Pterosauria (Reptilia) with soft parts with implications for pterosaurian anatomy and locomotion. In Evolution and Palaeobiology of Pterosaurs, E. Buffetaut, and J.-M. Mazin, eds. (Geological Society of London (Special Publications)), pp. 233–266. 217.
17. Tischlinger, H., and Frey, E. (2015). Flugsaurier (Pterosauria). In Solnhofen - Ein Fenster in die Jurazeit, G. Arratia, H.-P. Schultze, H. Tischlinger, and G. Viohl, eds. (Verlag Dr. Friedrich Pfeil), pp. 459–480.
18. Spindler, F. (2024). A pterosaurian connecting link from the Late Jurassic of Germany. Palaeontol. Electron. *27*, 1–27. https://doi.org/10.26879/1366.
19. Mateer, N.J. (1976). A statistical study of the genus *Pterodactylus*. Bull. Geol. Inst. Univ. Uppsala *6*, 97–105.
20. Bennett, S.C. (1995). A statistical study of *Rhamphorhynchus* from the Solnhofen Limestone of Germany: year-classes of a single large species. J. Paleontol. *69*, 569–580. https://doi.org/10.1017/S0022336000034946.
21. Bennett, S.C. (1996). Year-classes of pterosaurs from the Solnhofen Limestone of Germany: taxonomic and systematic implications. J. Vertebr. Paleontol. *16*, 432–444. https://doi.org/10.1080/02724634.1996.10011332.
22. Bennett, S.C. (2007). A review of the pterosaur *Ctenochasma*: taxonomy and ontogeny. N. Jahrb. Geol. Paläontol. Abh. *245*, 23–31. https://doi.org/10.1127/0077-7749/2007/0245-0023.
23. Bennett, S.C. (2013). New information on body size and cranial display structures of *Pterodactylus antiquus*, with a revision of the genus. Paläontologische Z. *87*, 269–289. https://doi.org/10.1007/s12542-012-0159-8.
24. Vidovic, S.U., and Martill, D.M. (2014). *Pterodactylus scolopaciceps* Meyer, 1860 (Pterosauria, Pterodactyloidea) from the Upper Jurassic of Bavaria, Germany: the problem of cryptic pterosaur taxa in early ontogeny. PLoS One *9*, e110646. https://doi.org/10.1371/journal.pone.0110646.
25. Vidovic, S.U., and Martill, D.M. (2018). The taxonomy and phylogeny of *Diopecephalus kochi* (Wagner, 1837) and '*Germanodactylus rhamphastinus*' (Wagner, 1851). In New Perspectives on Pterosaur Palaeobiology, D.W.E. Hone, M.P. Witton, and D.M. Martill, eds. (Geological Society), pp. 125–147.
26. Smyth, R.S.H., and Unwin, D.M. (2024). Re-evaluation of *Pterodactylus antiquus* and *Diopecephalus kochi*: two troublesome taxonomic concepts. J. Syst. Palaeontol. *22*, 1–35. https://doi.org/10.1080/14772019.2024.2421845.
27. Prondvai, E., Stein, K., Ősi, A., and Sander, M.P. (2012). Life history of *Rhamphorhynchus* inferred from bone histology and the diversity of pterosaurian growth strategies. PLoS One *7*, e31392. https://doi.org/10.1371/journal.pone.0031392.
28. Unwin, D.M., and Deeming, D.C. (2019). Prenatal development in pterosaurs and its implications for their postnatal locomotory ability. Proc. Biol. Sci. *286*, 20190409. https://doi.org/10.1098/rspb.2019.0409.
29. Naish, D., Witton, M.P., and Martin-Silverstone, E. (2021). Powered flight in hatchling pterosaurs: evidence from wing form and bone strength. Sci. Rep. *11*, 13130. https://doi.org/10.1038/s41598-021-92499-z.
30. Wang, X., Kellner, A.W.A., Jiang, S., Cheng, X., Wang, Q., Ma, Y., Paidoula, Y., Rodrigues, T., Chen, H., Sayão, J.M., et al. (2017). Egg accumulation with 3D embryos provides insight into the life history of a pterosaur. Science *358*, 1197–1201. https://doi.org/10.1126/science.aan2329.
31. Yang, Z., Jiang, B., Benton, M.J., Xu, X., McNamara, M.E., and Hone, D.W.E. (2023). Allometric wing growth links parental care to pterosaur gigantism. Proc. Biol. Sci. *290*, 20231102. https://doi.org/10.1098/rspb.2023.1102.
32. Foth, C., Brusatte, S.L., and Butler, R.J. (2012). Do different disparity proxies converge on a common signal? Insights from the cranial morphometrics and evolutionary history of Pterosauria (Diapsida: Archosauria). J. Evol. Biol. *25*, 904–915. https://doi.org/10.1111/j.1420-9101.2012.02479.x.
33. Chan, N.R. (2017). Morphospaces of functionally analogous traits show ecological separation between birds and pterosaurs. Proc. Biol. Sci. *284*, 20171556. https://doi.org/10.1098/rspb.2017.1556.
34. Navarro, C.A., Martin-Silverstone, E., and Stubbs, T.L. (2018). Morphometric assessment of pterosaur jaw disparity. R. Soc. Open Sci. *5*, 172130. https://doi.org/10.1098/rsos.172130.
35. Hone, D.W.E., Ratcliffe, J.M., Riskin, D.K., Hermanson, J.W., and Reisz, R.R. (2021). Unique near isometric ontogeny in the pterosaur *Rhamphorhynchus* suggests hatchlings could fly. Lethaia *54*, 106–112. https://doi.org/10.1111/let.12391.
36. Bestwick, J., Unwin, D.M., Butler, R.J., and Purnell, M.A. (2020). Dietary diversity and evolution of the earliest flying vertebrates revealed by dental microwear texture analysis. Nat. Commun. *11*, 5293. https://doi.org/10.1038/s41467-020-19022-2.
37. Wellnhofer, P. (2008). In *Archaeopteryx*Der Urvogel von Solnhofen (Verlag Dr. Friedrich Pfeil).
38. Barthel, K.W. (1978). Solnhofen – Ein Blick in die Erd-geschichte (Ott Verlag).
39. Barthel, K.W., Swinburne, N.H.M., and Conway Morris, S. (1990). Solnhofen: A Study in Mesozoic Palaeontology (Cambridge University Press).
40. Viohl, G. (2015). Der geologische Rahmen. In Solnhofen - Ein Fenster in die Jurazeit, G. Arratia, H.-P. Schultze, H. Tischlinger, and G. Viohl, eds. (Verlag Dr. Friedrich Pfeil), pp. 56–62.

41. Viohl, G. (2015). Die lithographischen Plattenkalke im engeren Sinne. In Solnhofen - Ein Fenster in die Jurazeit, G. Arratia, H.-P. Schultze, H. Tischlinger, and G. Viohl, eds. (Verlag Dr. Friedrich Pfeil), pp. 78–100.

42. Kemp, R.A. (2001). Generation of the Solnhofen tetrapod accumulation. Archaeopteryx *19*, 11–28.

43. Beardmore, S.R., Lawlor, E., and Hone, D.W.E. (2017). Using taphonomy to infer differences in soft tissues between taxa: an example using basal and derived forms of Solnhofen pterosaurs. Sci. Nat. *104*, 1–11.

44. Rauhut, O.W.M., López-Arbarello, A., Röper, M., and Rothgaenger, M. (2017). Vertebrate fossils from the Kimmeridgian of Brunn: the oldest fauna from the Solnhofen Archipelago (Late Jurassic, Bavaria, Germany). Zitteliana *89*, 305–329.

45. Schweigert, G. (2015). Biostratigraphie der Plattenkalke der südlichen Frankenalb. In Solnhofen - Ein Fenster in die Jurazeit, G. Arratia, H.-P. Schultze, H. Tischlinger, and G. Viohl, eds. (Verlag Dr. Friedrich Pfeil), pp. 63–66.

46. Munnecke, A., Westphal, H., and Kölbl-Ebert, M. (2008). Diagenesis of plattenkalk: examples from the Solnhofen area (Upper Jurassic, southern Germany). Sedimentology *55*, 1931–1946. https://doi.org/10.1111/j.1365-3091.2008.00975.x.

47. Keupp, H. (1977). The Solnhofen Lithographic Limestone—a laminite of coccoid blue-green algae. Paläontologische Z. *51*, 102–116. https://doi.org/10.1007/BF02986604.

48. Wang, X., and Zhou, Z. (2004). Palaeontology: Pterosaur embryo from the Early Cretaceous. Nature *429*, 621. https://doi.org/10.1038/429621a.

49. Ji, Q., Ji, S.A., Cheng, Y.N., You, H.L., Lü, J.C., Liu, Y.Q., and Yuan, C.X. (2004). Palaeontology: Pterosaur egg with a leathery shell. Nature *432*, 572. https://doi.org/10.1038/432572a.

50. Chiappe, L.M., Codorniú, L., Grellet-Tinner, G., and Rivarola, D. (2004). Palaeobiology: Argentinian unhatched pterosaur fossil. Nature *432*, 571–572. https://doi.org/10.1038/432571a.

51. Bennett, S.C. (1993). The ontogeny of *Pteranodon* and other pterosaurs. Paleobiology *19*, 92–106. https://doi.org/10.1017/S0094837300012331.

52. Bennett, S.C. (2006). Juvenile specimens of the pterosaur *Germanodactylus cristatus*, with a review of the genus. J. Vertebr. Paleontol. *26*, 872–878. https://doi.org/10.1671/0272-4634(2006)26[872:JSOTPG]2.0.CO;2.

53. Bennett, S.C. (2018). New smallest specimen of the pterosaur *Pteranodon* and ontogenetic niches in pterosaurs. J. Paleontol. *92*, 254–271. https://doi.org/10.1017/jpa.2017.84.

54. Codorniú, L., and Chiappe, L.M. (2004). Early juvenile pterosaurs (Pterodactyloidea: *Pterodaustro guinazui*) from the Lower Cretaceous of central Argentina. Can. J. Earth Sci. *41*, 9–18. https://doi.org/10.1139/e03-080.

55. Chinsamy, A., Codorniú, L., and Chiappe, L. (2008). Developmental growth patterns of the filter-feeder pterosaur, *Pterodaustro guinazui*. Biol. Lett. *4*, 282–285. https://doi.org/10.1098/rsbl.2008.0004.

56. Chinsamy, A., Codorniú, L., and Chiappe, L. (2009). Palaeobiological implications of the bone histology of *Pterodaustro guinazui*. Anat. Rec. (Hoboken) *292*, 1462–1477. https://doi.org/10.1002/ar.20990.

57. Manzig, P.C., Kellner, A.W.A., Weinschütz, L.C., Fragoso, C.E., Vega, C. S., Guimarães, G.B., Godoy, L.C., Liccardo, A., Ricetti, J.H.Z., and de Moura, C.C. (2014). Discovery of a rare pterosaur bone bed in a Cretaceous desert with insights on ontogeny and behavior of flying reptiles. PLoS One *9*, e100005. https://doi.org/10.1371/journal.pone.0100005.

58. Wang, X., Kellner, A.W.A., Jiang, S., Wang, Q., Ma, Y., Paidoula, Y., Cheng, X., Rodrigues, T., Meng, X., Zhang, J., et al. (2014). Sexually dimorphic tridimensionally preserved pterosaurs and their eggs from China. Curr. Biol. *24*, 1323–1330. https://doi.org/10.1016/j.cub.2014.04.054.

59. Kellner, A.W.A. (2015). Comments on Triassic pterosaurs with discussion about ontogeny and description of new taxa. An. Acad. Bras. Cienc. *87*, 669–689. https://doi.org/10.1590/0001-3765201520150307.

60. Codorniú, L., Chiappe, L., and Rivarola, D. (2018). Neonate morphology and development in pterosaurs: evidence from a ctenochasmatid embryo from the Early Cretaceous of Argentina. In New Perspectives on Pterosaur Palaeobiology, D.W.E. Hone, M.P. Witton, and D.M. Martill, eds. (Geological Society London Special Publications), pp. 83–94.

61. Dalla Vecchia, F.M. (2018). Comments on Triassic pterosaurs with a commentary on the "ontogenetic stages" of Kellner (2015) and the validity of *Bergamodactylus wildi*. Riv. Ital. Paleontol. Stratigrafia *124*, 317–341.

62. Codorniú, L., Chiappe, L.M., and Cid, F.D. (2013). First occurrence of stomach stones in pterosaurs. J. Vertebr. Paleontol. *33*, 647–654. https://doi.org/10.1080/02724634.2013.731335.

63. Lyman, R.L. (1994). Vertebrate Taphonomy (Cambridge University Press). https://doi.org/10.1017/CBO9781139878302.

64. Grodsky, S.M., Behr, M.J., Gendler, A., Drake, D., Dieterle, B.D., Rudd, R.J., and Walrath, N.L. (2011). Investigating the causes of death for wind turbine-associated bat fatalities. J. Mammal. *92*, 917–925. https://doi.org/10.1644/10-MAMM-A-404.1.

65. Jang, H.K., Park, J.M., Ahmed, S., Seok, S.H., Kim, H.S., and Yeon, S.C. (2019). Fracture analysis of wild birds in South Korea. J. Vet. Clin. *36*, 196–199. https://doi.org/10.17555/jvc.2019.08.36.4.196.

66. Padian, K. (1983). A functional analysis of flying and walking in pterosaurs. Paleobiology *9*, 218–239. https://doi.org/10.1017/S0094837300000765X.

67. Dumont, E.R. (2010). Bone density and the lightweight skeletons of birds. Proc. Biol. Sci. *277*, 2193–2198. https://doi.org/10.1098/rspb.2010.0117.

68. Beaufrère, H. (2009). A review of biomechanic and aerodynamic considerations of the avian thoracic limb. J. Avian Med. Surg. *23*, 173–185. https://doi.org/10.1647/2007-023.1.

69. Kim, T., and Kwon, Y. (2016). Bone fractures in raptors in the Daegu-Gyeongbuk region: a retrospective study. J. Vet. Clin. *33*, 261–265. https://doi.org/10.17555/jvc.2016.10.33.5.261.

70. Lovell, N.C. (1997). Trauma analysis in paleopathology. Am. J. Phys. Anthropol. *104*, 139–170.

71. Wood, H.B. (1941). Fractures among birds. Bird Banding *12*, 68–72. https://doi.org/10.2307/4509663.

72. Bennett, R.A., and Kuzma, A.B. (1992). Fracture management in birds. J. Zoo Wildl. Med. *23*, 5–38.

73. James, A.E., Montali, R.J., Novak, G.R., and Bush, M. (1978). The use of xeroradiographic imaging to evaluate fracture repair in avian species. Skelet. Rad. *2*, 161–168. https://doi.org/10.1007/BF00347315.

74. DiGeronimo, P.M., and Brandão, J. (2019). Orthopedics in reptiles and amphibians. Vet. Clin. North Am. Exot. Anim. Pract. *22*, 285–300. https://doi.org/10.1016/j.cvex.2019.01.009.

75. Romero, A.J., Díez, J.C., Rodríguez, L., and Arceredillo, D. (2016). Anthropic fractures and human tooth marks: An experimental approach to non-technological human action on avian long bones. Quat. Int. *421*, 219–227. https://doi.org/10.1016/j.quaint.2015.10.005.

76. Lloveras, L., Garcia, L., Marqueta, M., Maroto, J., Soler, J., and Soler, N. (2022). The role of birds in Upper Palaeolithic sites: Zooarchaeological and taphonomic analysis of the avian remains from Arbreda Cave (Serinyà, northeast Iberia). Quat. Int. *626–627*, 22–32. https://doi.org/10.1016/j.quaint.2020.10.022.

77. Kemp, R.A., and Trueman, C.N. (2003). Rare earth elements in Solnhofen biogenic apatite: geochemical clues to the palaeoenvironment. Sediment. Geol. *155*, 109–127. https://doi.org/10.1016/S0037-0738(02)00163-X.

78. Gerschermann, S., Ballhaus, C., and Gäb, F. (2021). Rheological properties of calcite oozes: Implications for the fossilisation in the plattenkalks of the Solnhofen-Eichstätt lagoons in the Franconian Alb, Germany. PLoS One *16*, e0252469. https://doi.org/10.1371/journal.pone.0252469.

79. Serrano, F.J., Costa-Pérez, M., Navalón, G., and Martín-Serra, A. (2020). Morphological disparity of the humerus in modern birds. Diversity *12*, 173. https://doi.org/10.3390/d12050173.

80. Biewener, A.A., and Dial, K.P. (1995). In vivo strain in the humerus of pigeons (*Columba livia*) during flight. J. Morphol. *225*, 61–75. https://doi.org/10.1002/jmor.1052250106.

81. Newton, I. (2007). Weather-related mass-mortality events in migrants. Ibis *149*, 453–467. https://doi.org/10.1111/j.1474-919X.2007.00704.x.

82. Wilson, A.K., Kurta, A., Kovacs, T., Westrich, B.J., Benavidez Westrich, K.M., and Kurta, R.M. (2023). Death on the beach: mass mortality of Eastern Red Bats over Lake Michigan. J. North American Bat Res. Notes *1*, 1–6.

83. Wiley, J.W., and Wunderle, J.M. (1993). The effects of hurricanes on birds, with special reference to Caribbean islands. Bird Conserv. Int. *3*, 319–349. https://doi.org/10.1017/S0959270900002598.

84. Nicoll, M.A.C., Nevoux, M., Jones, C.G., Ratcliffe, N., Ruhomaun, K., Tatayah, V., and Norris, K. (2017). Contrasting effects of tropical cyclones on the annual survival of a pelagic seabird in the Indian Ocean. Glob. Change Biol. *23*, 550–565. https://doi.org/10.1111/gcb.13324.

85. Trower, W. (1979). A wild goose storm disaster. Norfolk Bird & Mammal Report 25, pp. 102–104.

86. Schoombie, J., Schoombie, S., Connan, M., Jones, C.W., Risi, M., Craig, K.J., Smith, L., Ryan, P.G., and Shepard, E.L.C. (2023). Impact of wind on crash-landing mortality in grey-headed albatrosses *Thalassarche chrysostoma* breeding on Marion Island. Mar. Ecol. Prog. Ser. *723*, 213–225. https://doi.org/10.3354/meps14292.

87. Sell, R.A. (1917). Some Notes on the Effects upon Bird Life, of the Corpus Christi Storm of August 18, 1916. Condor *19*, 43–46. https://doi.org/10.2307/1362640.

88. Seys, J. (2001). Sea- and coastal bird data as tools in the policy and management of Belgian marine waters. PhD thesis (Ghent University).

89. Wolfaardt, A.C., Crofts, S., and Baylis, A.M. (2012). Effects of a storm on colonies of seabirds breeding at the Falkland Islands. Mar. Ornithol. *40*, 129–133. https://doi.org/10.5038/2074-1235.40.2.984.

90. Smith, K.T., Rabenstein, R., and O'Keefe, J. (2024). Was Palaeolake Messel a death-trap? Insight from modern bat drownings and decay experiments. Palaeobiodiversity Palaeoenvironments *104*, 977–997. https://doi.org/10.1007/s12549-024-00631-4.

91. Frey, E., and Martill, D.M. (1994). A new pterosaur from the Crato Formation (Lower Cretaceous, Aptian) of Brazil. N. Jahrb. Geol. Paläontol. Abh. *194*, 379–412. https://doi.org/10.1127/njgpa/194/1994/379.

92. Kemp, R.A., and Unwin, D.M. (1997). The skeletal taphonomy of *Archaeopteryx*: a quantitative approach. Lethaia *30*, 229–238. https://doi.org/10.1111/j.1502-3931.1997.tb00465.x.

93. Davis, P.G., and Briggs, D.E.G. (1998). The impact of decay and disarticulation on the preservation of fossil birds. Palaios *13*, 3–13. https://doi.org/10.2307/3515277.

94. Rhim, H., Gahng, J., Baek, G., Kim, M., and Han, J.I. (2024). Morbidity of rescued wild birds by admission causes in the Republic of Korea. Animals (Basel) *14*, 2071. https://doi.org/10.3390/ani14142071.

95. Hone, D.W.E., Tischlinger, H., Frey, E., and Röper, M. (2012). A new non-pterodactyloid pterosaur from the Late Jurassic of Southern Germany. PLoS One *7*, e39312. https://doi.org/10.1371/journal.pone.0039312.

96. Padian, K. (2008). The Early Jurassic pterosaur *Dorygnathus banthensis*. Spec. Pap. Palaeontol. *80*, 1–64.

97. Padian, K. (2008). The Early Jurassic pterosaur *Campylognathoides* Strand, 1928. Spec. Pap. Palaeontol. *80*, 65–107.

98. Unwin, D.M., and Martill, D.M. (2007). Pterosaurs of the Crato Formation. In The Crato Fossil Beds of Brazil, D.M. Martill, G. Bechly, and R.F. Loveridge, eds. (Cambridge University Press), pp. 475–524. https://doi.org/10.1017/CBO9780511535512.018.

99. Vila Nova, B.C., Saraiva, A.A.F., Moreira, J.K.R., and Sayão, J.M. (2011). Controlled excavations in the Romualdo Formation Lagerstätte (Araripe Basin, Brazil) and pterosaur diversity: remarks based on new findings. Palaios *26*, 173–179. https://doi.org/10.2110/palo.2010.p10-072r.

100. Etienne, J.L., Smith, R.E., Unwin, D.M., Smyth, R.S.H., and Martill, D.M. (2024). A 'giant' pterodactyloid pterosaur from the British Jurassic. Proc. Geol. Assoc. *135*, 335–348. https://doi.org/10.1016/j.pgeola.2024.05.002.

101. Butler, R.J., Benson, R.B.J., and Barrett, P.M. (2013). Pterosaur diversity: untangling the influence of sampling biases, Lagerstätten, and genuine biodiversity signals. Palaeogeogr. Palaeoclimatol. Palaeoecol. *372*, 78–87. https://doi.org/10.1016/j.palaeo.2012.08.012.

102. Dean, C.D., Mannion, P.D., and Butler, R.J. (2016). Preservational bias controls the fossil record of pterosaurs. Palaeontology *59*, 225–247. https://doi.org/10.1111/pala.12225.

103. Bennett, S.C. (2013). The morphology and taxonomy of the pterosaur *Cycnorhamphus*. N. Jahrb. Geol. Paläontol. Abh. *267*, 23–41. https://doi.org/10.1127/0077-7749/2012/0295.

104. Hone, D.W.E., Lauer, R., Lauer, B., and Spindler, F. (2023). *Petrodactyle wellnhoferi* gen. et sp. nov.: A new and large ctenochasmatid pterosaur from the Late Jurassic of Germany. Palaeontol. Electron. *26*, 1–28. https://doi.org/10.26879/1251.

105. Hone, D.W.E., Lauer, R., and Lauer, B. (2025). Soft tissue anatomy of pterosaur hands and feet–new information from Solnhofen region pterodactyloid specimens. Lethaia *58*, 1–12. https://doi.org/10.18261/let.58.3.1.

106. Schneider, C.A., Rasband, W.S., and Eliceiri, K.W. (2012). NIH Image to ImageJ: 25 years of image analysis. Nat. Methods *9*, 671–675. https://doi.org/10.1038/nmeth.2089.

107. Hammer, Ø., Harper, D.A.T., and Ryan, P.D. (2001). PAST: Paleontological Statistics Software Package for Education and Data Analysis. Palaeontol. Electron. *4*, 1–9.

108. Martill, D.M., and Naish, D. (2006). Cranial crest development in the azhdarchoid pterosaur *Tupuxuara*, with a review of the genus and tapejarid monophyly. Palaeontology *49*, 925–941. https://doi.org/10.1111/j.1475-4983.2006.00575.x.

Please cite this article in press as: Smyth et al., Fatal accidents in neonatal pterosaurs and selective sampling in the Solnhofen fossil assemblage, Current Biology (2025), https://doi.org/10.1016/j.cub.2025.08.006

STAR★METHODS

KEY RESOURCES TABLE

REAGENT or RESOURCE	SOURCE	IDENTIFIER
Other		
Pterodactylus antiquus	Bürgermeister-Müller-Museum, Solnhofen (BMMS); Museum Bergér (MBH); Bavarian State Collection for Palaeontology and Geology (SNSB-BSPG); Teylers Museum (TM)	BMMS uncat. (Figure 5D); MBH 250624-07 (Figures 1A, 1B, 3A, and 3B); MBH 250624-09 (Figure 5E); MBH 250624-10 (Figure 5F); SNSB-BSPG 1937 I 18 (Figure 5B); SNSB-BSPG 1993 XVIII 1508 (Figures 1C, 1D, and 3C); SNSB-BSPG AS I 739 (Figure 5C); TM 13105 (Figure 5A)
Deposited data		
Pterodactylus antiquus morphometric, stratigraphic, and taphonomic data	Wellnhofer[1]; Smyth and Unwin[26]; this paper	Data S1A
Pterodactylus antiquus skull length estimates	This paper	Data S1B
Ontogenetic assessment of pterosaur embryonic and neonatal specimens	Wellnhofer[1]; Bennett[20,21,51–53]; Prondvai et al.[27]; Unwin and Deeming[28]; Wang and Zhou[48]; Ji et al.[49]; Chiappe et al.[50]; Codorniú and Chiappe[54]; Chinsamy et al.[55,56]; Manzig et al.[57]; Wang et al.[58]; Kellner[59]; Codorniú et al.[60]; Dalla Vecchia[61]; this paper	Data S1C
Pterodactylus antiquus skeletal completeness data	This paper	Data S1D
Pterodactylus antiquus skeletal articulation data	This paper	Data S1E
Ctenochasmatoid morphometric, stratigraphic, and taphonomic data	Wellnhofer[1]; Bennett[22,103]; Hone et al.[104,105]; this paper	Data S1F
Rhamphorhynchus muensteri morphometric, stratigraphic, and taphonomic data	Wellnhofer[2]; Hone et al.[35]; this paper	Data S1G
Software and algorithms		
ImageJ v1.53u	Schneider et al.[106]	https://imagej.net/ij/
Past v4.17	Hammer et al.[107]	https://www.nhm.uio.no/english/research/resources/past/

EXPERIMENTAL MODEL AND SUBJECT DETAILS

The two new specimens of *Pterodactylus* documented for this study are housed in the following institutions: Museum Bergér, Harthof (MBH) and the Bavarian State Collection for Palaeontology and Geology, Munich (SNSB-BSPG). Metric data for other Solnhofen pterosaurs were taken from the published literature. See Data collection section below and Data S1 for more information.

METHOD DETAILS

Data Collection

Specimens were examined using standard methods including visual inspection, binocular microscopy and photography using regular and low- angled illumination, and UV fluorescence. Photography was conducted using a Nikon D850, UV (Hoya UV(0)) and polarizing filters. Light sources included natural light, tungsten lamps and hand-held UV LED lamps (Weltool M2-BF; wavelength 365 nm;

Please cite this article in press as: Smyth et al., Fatal accidents in neonatal pterosaurs and selective sampling in the Solnhofen fossil assemblage, Current Biology (2025), https://doi.org/10.1016/j.cub.2025.08.006

LED radiation flux 2100 microwatts). The following camera settings were used to eliminate vibration during relatively long exposures: mirror locked up; shutter release delay five seconds; support of specimens using a rubber mat.

Ultraviolet Fluorescence Photography (UVFP) revealed evidence of the original condition of the limestone plate upon which the specimen is borne and skeletal features that are difficult to discern using natural light, including bone to bone sutures in the skull, and fine detail of individual skeletal elements (including texture and bone wall thickness). UVFP also revealed areas of soft tissue preservation that are barely visible in normal light, including articular calcified cartilage and wing membrane impression associated with the left wing-finger in MBH 250624-07.

Metric data for pterosaurs was obtained by direct measurement of specimens, as well as from scaled photographs using ImageJ v.1.53u.[106] Additional data for Solnhofen pterosaurs was taken from existing measurements and data sets.[1,2,22,26,35,103–105]

QUANTIFICATION AND STATISTICAL ANALYSIS

Body size estimates

Skull length was chosen as a proxy for overall body size as it is one of the most frequently preserved elements and even in examples where the total length of the skull could not be calculated it could usually be estimated from another cranial measurement which shows a high degree of correlation with skull length. For *P. antiquus*, skull length estimates were derived from prenarial rostrum length ($r^2 = 0.98$) (Figure S1A); skull height ($r^2 = 0.98$) (Figure S1B); or mandible length ($r^2 = 0.99$) (Figure S1C). In rare instances where none of these cranial data were preserved skull length estimates were determined based on the preserved element that most strongly correlated with skull length: wing phalanx 2 length ($r^2 = 0.98$) (Figure S1D); or femur length ($r^2 = 0.97$) (Figure S1E).

Skull length was used as a proxy for body size in other Solnhofen pterosaur groups. For ctenochasmatoid specimens that lacked a complete skull, estimates were calculated from humerus length ($r^2 = 0.99$) (Figure S2A); radius length ($r^2 = 0.97$) (Figure S2B); wing phalanx 1 length ($r^2 = 0.97$) (Figure S2C); femur length ($r^2 = 0.97$) (Figure S2D); tibia length ($r^2 = 0.96$) (Figure S2E); or were taken from the literature.[1,22] Similar methods were used to estimate skull lengths for several *Rhamphorhynchus* specimens. These were calculated using tail length ($r^2 = 0.96$) (Figure S3A); humerus length ($r^2 = 0.92$) (Figure S3B); wing phalanx 1 length ($r^2 = 0.94$) (Figure S3C); wing phalanx 2 length ($r^2 = 0.92$) (Figure S3D); wing phalanx 3 length ($r^2 = 0.90$) (Figure S3E); or femur length ($r^2 = 0.90$) (Figure S3F).

Ontogenetic assessment

To examine the developmental stage of the smallest specimens of *Pterodactylus*, a comparative analysis was conducted on the degree of ossification across seven *Pterodactylus* individuals. This was calibrated using known examples of embryonic and neonates of other pterosaur taxa to assess developmental trajectories in skeletogenesis (Figure 2B; Data S1) modified from Unwin & Deeming.[28]

The pterosaur skeleton was subdivided into a series of discrete structural units, each evaluated separately for: ossification stage, bone surface texture, and element fusion (where applicable). Ossification categories included: unossified (no visible mineralisation); poorly ossified (partial ossification, typically restricted to the mid-diaphysis); and well ossified (complete ossification). To accommodate incomplete preservation and taphonomic loss, missing or indeterminate data were coded as unknown ("?").

Bone texture was scored as an independent character and refers to the surface condition of ossified elements, reflecting the maturity of the forming bone. The categories were: extensive fibrous texture (coarse, striated bone surface indicative of early-stage mineralisation); limited fibrous texture (fine or patchy fibrous surface, suggesting intermediate development); and absent fibrous texture (smooth, dense bone surface typical of more mature ossified tissue).

Fusion of skeletal elements was also treated as a discrete character, applied to compound structures such as vertebrae, girdle elements, and limb epiphyses. Fusion states included: separate, partially co-ossified, fully co-ossified.

The following characters were used to capture key developmental features:

1. Principal cranial elements: unossified (0), partially ossified (1), fully ossified (2).
2. Mandible elements: unossified (0), partially ossified (1), fully ossified (2).
3. Elongate elements of the cranium exhibit a 'fibrous' texture: extensive (0), limited (1), absent (2).
4. Principal appendicular elements exhibit a 'fibrous' texture: extensive (0), limited (1), absent, surface texture smooth and dense (2).
5. Principal cranial elements: separate (0), some elements partially co-ossified (1); most/all elements co-ossified (2).
6. Centrum and neural arch of cervical vertebrae: separate (0), partially co-ossified (1); fully co-ossified (2).
7. Centrum and neural arch of dorsal vertebrae: separate (0); partially co-ossified (1); fully co-ossified (2).
8. Sacral vertebrae: separate (0), partially co-ossified (1); fully co-ossified (2).
9. Sacral ribs, sacral vertebrae and ilium: separate (0), partially co-ossified (1); fully co-ossified (2).
10. Caudal vertebrae: unossified (0); partially ossified (1); fully ossified (2).
11. Scapula and coracoid: separate (0), partially co-ossified (1); fully co-ossified (2).
12. Sternum: unossified (0), partially ossified (1), fully ossified (2).
13. Humerus and distal epiphyses: epiphyses unossified (0); epiphyses partially/fully ossified but separate from diaphysis (1); epiphyses fully ossified and fused with diaphysis (2).
14. Carpals: unossified (0), partially ossified (1), fully ossified (2).
15. Radiale and ulnare: separate elements (0), partially co-ossified (1); fully co-ossified (2).

16. Distal carpals: separate elements (0), partially co-ossified (1); fully co-ossified (2).
17. Wing phalanx 1 and extensor tendon process: separate (0); partially co-ossified (1); fully co-ossified (2).
18. Ilium, ischium and pubis: separate (0); partially co-ossified (1); fully co-ossified (2).
19. Tibia and fibula: separate (0), partially co-ossified (1) fully co-ossified (2).
20. Tarsals: unossified (0), partially ossified (1), fully ossified (2).
21. Proximal tarsals and tibia: separate (0); partially co-ossified (1); fully co-ossified (2).
22. Intermediate phalanges (IV-2 and IV-3) of pedal digit four: unossified (0); partially ossified (1); fully ossified (2).

Quantitative taphonomy

To analyse the taphonomic profile of *Pterodactylus antiquus*, we examined 48 specimens. Of these, seven specimens had to be excluded from the analysis. Two of these specimens (Wellnhofer Nos. 18 and 19) are lost,[1] and we could not locate any casts or photographs to assess their preservation. Other excluded specimens (SNSB-BSPG 1929 I 18, JME-SOS 2478, JME-SOS 4588, MBH 250624-12) are highly incomplete due to being preserved on broken slabs. Because the edges of the slabs intersect with the specimens, it is impossible to determine whether the missing material results from taphonomic processes or from incomplete collection of the specimens. Body size classes were defined using skull length as a proxy for overall size.[20,21,53] Skull lengths, including both measured and estimated values, were analysed to identify the abundance of various size classes. Kernel density estimation (KDE) was applied to the data using a Gaussian kernel, providing a smoothed representation of the distribution and aiding in the determination of meaningful size class boundaries.

Skeletal completeness was calculated by scoring a set of individual anatomical units and grouped anatomical units as present (1), absent (0), or unidentifiable (?), for each specimen included. Unidentifiable units (?) were those which might reasonably be assumed to be present but were not observable, for example if obscured by another unit, and therefore may be either present or absent. In the case of grouped units, the presence of any unit from within the group would give a present score (i.e. 1).

Individual units: Skull; Mandible; Sternum; Scapula (L); Coracoid (L); Scapula (R); Coracoid (R); Humerus (L); Radius/ulna (L); Metacarpal IV (L); Manus IV 1 (L); Manus IV 2 (L); Manus IV 3 (L); Manus IV 4 (L); Pteroid (L); Humerus (R); Radius/ulna (R); Metacarpals (R); Metacarpal IV (R); Manus IV 1 (R); Manus IV 2 (R); Manus IV 3 (R); Manus IV 4 (R); Carpus (R); Pteroid (R); Manus I (L); Manus II (L); Manus III (L); Manus I (R); Manus II (R); Manus III (R); Pelvis; Prepubis (L); Prepubis (R); Femur (L); Tibia fibula (L); Femur (R); Tibia fibula (R).

Grouped units: Metacarpals (L); Carpus (L); Cervicals; Dorsal-sacrals; Caudals; Ribs; Gastralia; Tarsus (R); Tarsus (L); Pedal V (R); Pedal V (L); Metatarsals (L); Pedal I (L); Pedal II (L); Pedal III (L); Pedal IV (L); Pedal (L); Metatarsals (R); Pedal I (R); Pedal II (R); Pedal III (R); Pedal IV (R); Pedal V (R).

Skeletal articulation was calculated by scoring a set of joints within each specimen as articulated (2), associated (1), and disarticulated (0). Joints were scored as articulated (2) when any part of the articulatory surfaces were in contact. Joints were scored as associated (1) when the articulatory surfaces were not in contact but were separated by less than 20% of the larger element's length. Joints were scored as disarticulated if the articulatory surfaces were greater than 20% of the larger element's length apart; this includes joints where only one element is present. In grouped joints, the score was based on the highest score for any articulation within the group.

Individual joints

Skull/mandible; Skull/cervical; Cervical/dorsal; Coracoid/sternum (L); Scapula/coracoid (L); Coracoid/sternum (R); Scapula/coracoid (R); Scapulocoracoid/humerus (L); Humerus/ulna (L); Metacarpal IV/manus IV 1 (L); Manus IV I/manus IV 2 (L); Manus IV 2/manus IV 3 (L); Manus IV 3/manus IV 4 (L); Scapulocoracoid/humerus (R); Humerus/ulna (R); Metacarpal IV/manus IV 1 (R); Manus IV I/manus IV 2 (R); Manus IV 2/manus IV 3 (R); Manus IV 3/manus IV 4 (R); Femur/tibia (L); Femur/tibia (R); Metatarsal I/pes I (L); Metatarsal II/pes II (L); Metatarsal III/pes III (L); Metatarsal IV/pes IV (L); Metatarsal I/pes I (R); Metatarsal II/pes II (R); Metatarsal III/pes III (R); Metatarsal IV/pes IV (L); Pelvis/femur (L); Pelvis/femur (R).

Grouped joints

Cervical/cervical; Dorsal/dorsal; Caudal/caudal; Carpus/radius/pteroid (L); Ulna/carpus (L); Carpus/metacarpal IV (L); Ulna/carpus (R); Carpus/MCIV (R); Radius/carpus/pteroid (R); Manus I/manus I (L); Manus II/manus II (L); Manus III/Manus III (L); Manus I/manus I (R); Manus II/manus II (R); Manus III/manus III (R); Tarsus or metatarsals/pes V (L); Tarsus or metatarsals/pes V (R); Tibia/tarsus (L); Tarsus/metatarsals (L); Pes I/pes I (L); Pes II/pes II (L); Pes III/pes III (L); Pes IV/pes IV (L); Tibia/tarsus (R); Tarsus/metatarsal (R); Pes I/pes I (R); Pes II/pes II (R); Pes III/pes III (R); Pes IV/pes IV (R). In both completeness and articulation units, L and R refer to the left and right of the specimen respectively, as observed from dorsal view.

Relative completeness scores were calculated by dividing the number of observed anatomical units by the maximum possible number of taxonomic units (excluding units whose presence or absence could not be determined). Likewise, relative articulation scores were determined by dividing the sum of observed articulations and associations by the maximum possible articulation score. To avoid compounding relative articulation scores with completeness, joints for which no contributing element was present were excluded from possible articulation scores. Analyses comparing body size (represented by skull length) with relative completeness and articulation were conducted in Past 4.17,[107] with non-linear regressions fitted using logistic models. The logistic curve provided a

Please cite this article in press as: Smyth et al., Fatal accidents in neonatal pterosaurs and selective sampling in the Solnhofen fossil assemblage, Current Biology (2025), https://doi.org/10.1016/j.cub.2025.08.006

strong fit for completeness ($r^2 = 0.71$) but a weaker fit for articulation ($r^2 = 0.37$). This discrepancy likely arises from biases inherent in the calculation of relative articulation. For example, articulation scores cannot reliably account for highly incomplete specimens, such as isolated limbs. An isolated but otherwise fully articulated forelimb, for example, preserves only a single point of disarticulation so may receive a disproportionately high relative articulation score simply due to the unknown fate of the rest of the skeleton. As a result, articulation scores can overestimate the articulation of some specimens, leading to a weaker observed fit.

Degrees of completeness and articulation in individual specimens of *P. antiquus*, ctenochasmatoids and *Rhamphorhynchus muensteri* were compared using established preservation categories.[1] Each specimen was classified according to the following types:

Type 1: Complete skeletons with bones in natural, life-like articulation.
Type 2: Disarticulated skeletons:
a: Some elements disarticulated, but overall retaining a life-like arrangement.
b: Scattered skeletal elements distributed across the deposit.
Type 3: Isolated skeletal elements with no associated or articulated components.

Given the degree of subjectivity in distinguishing between Type 2a and 2b specimens, Type 2 was treated as a single category.

Taxonomic assignment of incomplete specimens: MBH 250624-09, MBH 250624-10, MBH 250624-11, MBH 250624-12, LF 2314P/LF 3398N

Despite consisting only of isolated rostra (premaxilla + maxilla), MBH 250624-09 and MBH 250624-10 can be referred to *Pterodactylus antiquus* based on a combination of features that do not co-occur in any other species of Solnhofen pterosaur. These include an elongate rostrum (rostral index[108] between 6.0-8.0), with a slightly concave dorsal margin. Flat, conical, orthodont dentition, with tooth crowns about twice as long as their basal width, extending to the jaw tip and decreasing in size posteriorly. Three teeth are present in each premaxilla, with 16-17 teeth (excluding replacement teeth) in the prenarial portion of the upper tooth row.

Two specimens consisting only of forelimb elements, MBH 250624-11 and MBH 250624-12, are referred to *P. antiquus* based on the following combination of features: wing phalanx 2 length ~93% of wing phalanx 1 length; manual phalanx III-3 slightly shorter than manual phalanx III-1; manual unguals between 60-80% of their preceding phalanges.

A recently described isolated hindlimb (LF 2314P/LF 3398N) with exceptional soft tissue preservation of the pes was provisionally assigned to *Germanodactylus cristatus*, based on pronounced femoral curvature and a high tibia-to-femur ratio (1.6).[105] However, pedal morphology does not support this assignment. The specimen displays elongated proximal and shortened penultimate phalanges, particularly in digits III and IV (pph III-3/III-1 = 0.6; pph IV-4/IV-1 = 0.5). In *G. cristatus* (SMNK PAL 6592), these ratios are more equal (pph III-3/III-1 ~1.0; pph IV-4/IV-1 = 0.7). Among Solnhofen pterosaurs, such pedal proportions are so far only known in ctenochasmatoids, leading us to assign LF 2314P/LF 3398N as an indeterminate ctenochasmatoid. The features originally used to associate it with *G. cristatus* are likely ontogenetically variable and reflect the large size of the *G. cristatus* holotype. Notably, the femoral curvature in LF 2314P/LF 3398N resembles that of a large specimen of *P. antiquus* (Figure 5D) that is less well-developed in smaller individuals.